

弘前大学修士学位論文

Boosting production of formic acid from carbon dioxide

electroreduction via high-entropy material

高エントロピー材料を用いた二酸化炭素電気化学還元による

蟻酸の生産

弘前大学大学院地域共創科学研究科修士前期課程

地域リノベーション専攻

周 奕帆 (ZHOU YIFAN)

2024年01月31日

Contents

ABSTRACT	1
Chapter One.....	3
Introduction	3
1.1 Research Background	3
1.2 Electrochemical CO ₂ RR to Formic Acid	4
1.2.1 CO ₂ RR to Value-added Chemicals and Fuels	5
1.2.2 Foundation of Electrochemical CO ₂ RR.....	8
1.2.3 Mechanism of CO ₂ RR to Formic Acid.....	11
1.2.4 Electrolyte of electrochemical CO ₂ RR.....	14
1.2.5 Operational Parameters of electrochemical CO ₂ RR.....	14
1.3 Electrocatalysts for CO ₂ RR to Formic Acid.....	16
1.3.1 Bi-based catalysts.....	16
1.3.2 In-based catalysts.....	18
1.3.3 Sn-based catalysts	19
1.3.4 Pb-based catalysts.....	19
1.3.5 Cu-based catalysts	20
1.4 High-entropy materials	20
1.4.1 Structural features of HEMs	22
1.4.2 Four core effects.....	23
1.4.3 Synthesis of HEMs.....	25
1.4.4 Characterization	29

1.5 Anode reaction: Oxygen reduction reaction	31
1.5.1 Fundamental of OER.....	31
1.5.2 Oxygen evolution reaction and chlorine evolution reaction	33
1.5.3 HEM electrocatalysts for OER	33
Chapter Two	36
Experimental Materials and Test Methods.....	36
2.1 Experimental materials	36
2.2 Experimental equipment	37
2.3 Characterization methods and testing methods	37
2.3.1 X-ray Diffraction Analysis (XRD)	37
2.3.2 Scanning Electron Microscopy (SEM)	38
2.3.3 X-ray energy dispersive spectroscopy (EDX)	38
2.3.4 Transmission electron microscopy (TEM)	39
2.3.5 Electrochemical test	39
2.3.6 High-performance liquid chromatography (HPLC).....	40
Chapter Three	42
Formation of high entropy metal organic frameworks cathode for promoting carbon dioxide reduction reaction to formic acid.....	42
3.1 Introduction.....	42
3.2 Experimental	43
3.2.1 Nickel Foam Treatment	44
3.2.2 Precursor Deposition on NiF (Hydrothermal Method).....	44
3.3 Result and discussion	44

3.3.1 Morphology and crystal structure	44
3.3.2 Electrochemical test.....	46
3.3.3 conclusion	46
Chapter Four	48
Formation of high entropy oxide anode by morphology remodeling for promoting oxygen evolution reaction	48
4.1 Introduction	48
4.2 Experimental.....	49
4.2.1 Nickel Foam Treatment.....	49
4.2.2 Precursor Deposition on NiF (Hydrothermal Method)	49
4.2.3 Conversion to high-entropy oxide (HEO).....	50
4.3 Result and discussion	50
4.3.1 Morphology and crystal structure	50
4.3.2 The influence of composition on the morphologies and crystals	52
4.3.3 Electrochemical test.....	53
4.3.5 conclusion	54
Chapter Five	56
General conclusion	56
Reference.....	57
Acknowledgements.....	73
List of publications and presentations.....	75

ABSTRACT

Excessive carbon dioxide emissions have brought about serious resource, environmental, and climate issues. Therefore, converting CO₂ into valuable chemical fuels has attracted increasing research attention. As one of the most attractive CO₂ reduction products, formic acid (HCOOH) is widely considered an ideal hydrogen carrier. Due to intense competitive hydrogen evolution reaction (HER) in aqueous media, high applied potential as well as current density often leads to low Faradaic efficiency (FE). Therefore, achieving a low-cost, environmentally friendly, and highly active catalyst to promote the generation of HCOOH by reducing CO₂ in aqueous solutions with high current density and FE is of great interest but remains a challenge. Additionally, the carbon dioxide reduction reaction is always combined with the oxygen evolution reaction (OER), therefore, the development of efficient OER electrocatalysts is also important and sometimes it becomes the main obstacle to affect the efficiency of overall electrochemical process.

This study focuses on the applications of high-entropy materials (HEMs) as either cathode or anode electrocatalysts in electrochemical CO₂ reduction reaction (CO₂RR). Here, HEMs always consist of five or more primary elements with close atomic ratios ranged from 5~35 at% for each. These usually offer adjustable composition, optimal grain size, stable crystalline structure, modified bond length and good electron cloud distribution, endowing HEMs long-term stability and unexcepted catalytic performance. Moreover, the complex components and structure of HEMs could result in discrepant atomic distribution and special binding sites, which can modulate the binding energy of reactants in a continuous form by varying elemental ratio. Unfortunately, as of now, there have been no reports of high-entropy catalysts that can be used to produce formic acid effectively from CO₂.

Herein, we chose Bi, In, Sn, Pb, and Cu five elements with carbon paper (CP) as the substrate and synthesized a catalyst by a simple hydrothermal method. XRD and elemental analysis confirmed the formation of a high-entropy structure of BiInSnPbCu on the CP. The obtained electrocatalyst exhibited high selectivity (over 80% Faradaic efficiency) and stability in electrochemical CO₂RR to formic acid. Meanwhile, a kind of high-entropy precursor with a fusiform microstructure was used to prepare high entropy oxide (HEO) of (FeCoNiMnCu)O_x for OER. It is observed that, with thermal oxidization, the morphology of obtained high-entropy (FeCoNiMnCu)O_x was conversed to layered sphere-shape microstructure built by nanodots. This HEO also showed excellent stability with running continuously for 160 hours at current densities even exceeding 100 mA cm⁻², which surpassed the performances of precious metal based electrocatalysts. Due to the excellent performances of the above obtained CO₂RR and OER high entropy electrocatalysts, it is expected to combine them to achieve efficient CO₂RR-OER electrolysis.

Chapter One

Introduction

1.1 Research Background

Since the onset of the industrial revolution, the widespread dependence on fossil fuels has led to a rapid increase in the concentration of carbon dioxide (CO₂) in the Earth's atmosphere. Starting at 280 parts per million (ppm) in 1750, the global CO₂ concentration reached 415 ppm in 2021 [1], triggering various environmental challenges, including global warming and ocean acidification. As of the latest data, the atmospheric CO₂ concentration stands at approximately 416.39 ppm, signifying a remarkable 46% increase from the pre-industrial era. The ramifications of this escalating CO₂ concentration are manifold, contributing to the intensification of climate change and the acidification of oceans, with far-reaching consequences for ecosystems and biodiversity. Recognizing the urgency of addressing this critical issue, global bodies such as the Intergovernmental Panel on Climate Change (IPCC) and the United Nations Climate Change Conference have stressed the critical need to limit CO₂ emissions. The IPCC emphasized the pressing need to reduce CO₂ emissions by a substantial margin—specifically, by at least half of the current emission levels—by the year 2050. This ambitious target is set with the overarching goal of averting further detrimental impacts associated with the ongoing rise in global average temperature. The scientific consensus underscores that such emission reduction efforts are essential to mitigate the severity of climate change, preserve ecological balance, and ensure the sustainability of the planet for future generation [2].

Reducing CO₂ emissions, carbon capture utilization and storage are three effective ways to reduce CO₂ concentration. The primary pathway to reduce CO₂ emissions at the source is through the substitution of renewable energy sources including sunlight, waves, wind, biomass, geothermal energy and nuclear energy for fossil fuels. These renewable energy sources have the capability to

generate electricity without releasing CO₂ emissions. Due to the temporal and geographical variations of these energy sources, achieving a sustainable and consistent utilization is challenging. Converting them into environmentally friendly fuels that can be stored is a viable solution. However, there are still many challenges in the storage, transportation, and utilization of these energy, making it difficult to effectively reduce CO₂ emissions at the source. An alternative and practical approach for mitigation involves storage. Generally, CO₂ is stored over the long term in subsurface rock formations through mineral carbonation, oceanic injection, or geological injection. Nevertheless, this method comes with limitations including high costs, substantial energy requirements for pumping and separation, and CO₂ storage on-site durability. In addition, storage of CO₂ faces risks of site leakage and groundwater contamination [3]. Therefore, CO₂ storage cannot provide a permanent solution and also cannot help solving future energy needs. Therefore, one of the most immediate challenges is determining how to effectively harness the potential of CO₂.

1.2 Electrochemical CO₂RR to Formic Acid

CO₂ stands as the predominant greenhouse gas, however, it wields the potential to undergo transformative processes to give rise to value-added fuels. This capability serves as a crucial step toward reducing our reliance on conventional fossil fuels. Moreover, the utilization and conversion of CO₂ offer a multifaceted approach to addressing the various challenges posed by global warming. Reducing the human-induced levels of atmospheric CO₂ and converting it into valuable raw materials using cost-effective and environmentally friendly techniques opens the path to establishing a sustainable chemical industry and energy economy [4].

Remarkably, CO₂ is characterized by its thermodynamic stability, with a Gibbs free energy change (ΔG) of approximately -394 kJ/mol. It exists as molecule, featuring two double bonds and displaying ultralow reactivity. Overcoming the thermodynamic barrier for its activation becomes a formidable challenge. Successfully converting CO₂ through chemical pathways and achieving its economical utilization demands significant technological and scientific efforts.

1.2.1 CO₂RR to Value-added Chemicals and Fuels

The conversion of CO₂ can be accomplished through various methods, including biochemical, thermochemical, photochemical, or electrochemical processes (Table 1.1).

Table 1.1 Possible products from CO₂ conversion.

Technology	Product	Reference
	Carbon monoxide	5
	Ethanol	6
Biochemical conversion	Isoprene	6
	Isobutanol	6
	Bio-plastics	5
	Carbon monoxide	7
Thermochemical conversion	Methanol	7
	Ethylene	7
	Carbon monoxide	12
	Methane	14
	Formic acid	15
Photochemical conversion	Methanol	16
	Ethane	17
	Cyclohexanol	18
	Cyclohexyl formate	18
Electrochemical conversion	Carbon monoxide	19
	Formic acid	20
	Methanol	21
	Ethanol	22
	Ethylene	22

Acetone	23
Acetic acid	23
Oxalic acid	24

Biochemical conversions have gained prominence as the viable approach for CO₂ reduction, primarily owing to their high efficiency, selectivity, substantial yields, minimal waste generation, and the ability to utilize low-purity reactants. It involves enzyme-catalyzed transformations of CO₂, with notable examples being the catalysis of CO₂ to carbon monoxide by carbon monoxide dehydrogenase [5]. The key to successful biochemical conversion lies in cultivating and engineering bacteria or algae equipped with specific conversion enzymes. This enables the efficient and large-scale transformation of CO₂ into valuable products. For instance, engineered bacteria have demonstrated the capability to produce ethanol, isoprene, and isobutanol through these enzymatic processes [6]. Another noteworthy example involves methanotrophic bacteria, which capture CO₂ and convert it into valuable products. This microorganism stores the CO₂ as polyhydroxyalkanoates (PHA), commonly recognized as bio-plastics [5]. However, the high cost associated with enzyme modification through genetic engineering poses an economic barrier to large-scale implementation. Additionally, the response times in bioconversion processes tend to be longer compared to traditional strategies, limiting their competitiveness in certain industrial applications. Furthermore, algae and bacteria have strict environmental and climatic requirements, which further limits the geographical applicability of this method.

Thermal catalytic CO₂ conversion involves using catalysts and high temperatures to facilitate the transformation of CO₂ [7]. The high stability and inert nature of CO₂ molecules make direct dissociation thermodynamically unfavorable. Therefore, decomposing of CO₂ to CO requires high temperature and active catalysts. Currently, the efficiency of direct decomposition of CO₂ is still very low (only 10% CO₂ conversion to CO and O₂), and the products, CO and O₂, are difficult to separate directly, making it challenging for industrial applications [8]. On an industrial scale, approximately 70 million metric tons of CH₃OH are produced annually through the selective

hydrogenation of CO₂. A significant hurdle in methanol production lies in the generation of H₂O, with one-third of the hydrogen being wasted in the production of H₂O [9]. CO₂ is commonly transformed into CH₄ through the Sabatier-Senderens reaction, commonly known as CO₂ methanation. This process stands out for its highly favorable attributes, characterized by a negative enthalpy and Gibbs free energy of -130.8 kJ/mol. Despite the thermodynamic favorability of the Sabatier-Senderens reaction, which is underscored by the negative enthalpy and Gibbs free energy values, its kinetic feasibility encounters limitations. The intricacy arises from the involvement of eight participating electrons in the process, creating a challenge in terms of electron transfer kinetics. This complexity hampers the efficiency of the methanation reaction under standard conditions [10]. The use of high temperature is a characteristic feature of thermalcatalytic reactions while they are essential for promoting reaction kinetics and efficiency. They also raise potential risks and challenges related to safety. Moreover, the presence of flammable or reactive substances in thermal catalytic reactions adds another layer of complexity to safety considerations. Therefore, thermal catalysis is not the optimal method for CO₂ reduction.

Photocatalytic conversion of CO₂ emerges as an innovative and sustainable technology utilizing light irradiation to reduce CO₂. This approach has gained considerable attention for its distinct advantages, including operating under moderate pressure, low temperatures, and without the need for excessive input energy. Photocatalysis relies on harnessing light energy to drive chemical reactions through a photocatalyst, involving key steps of light absorption, charge separation and transfer, and subsequent surface catalytic reactions [11]. The efficiency of CO₂ conversion, as well as the yield and selectivity of products, are primarily determined by the photocatalyst in this process.

Research indicates that the highest yield in the photocatalytic reduction of CO₂ results in CO, with a production rate as high as 7600 μmol/g/s when using Rh-Au/SBA-15 as the catalyst [12]. However, the noble metal catalysts face the challenge of high cost and limited scalability. While some non-precious metal catalysts can generate high-value products like carbon monoxide [13], methane [14], formic acid [15], methanol [16], ethane [17], cyclohexanol and cyclohexyl formate [18], their low production rates make it challenging for large-scale applications. Additionally, the

widespread commercial adoption of photocatalysis technology on a large scale is impeded by the constrained stability and efficiency of catalytic materials, compounded by the inherent instability of sunlight.

Electrochemical conversion offers notable advantages in terms of required operating conditions, making it a promising avenue for reducing atmospheric CO₂ concentration. Currently, electrocatalytic CO₂ reduction has been applied in the synthesis of various compounds (Table 1.1), including carbon monoxide [19], formic acid [20], methanol [21], ethylene, ethanol [22], acetic acid, acetone [23], and oxalic acid [24]. One of the key benefits of this way is the ability to take place at ambient temperature and pressure. This feature enhances the feasibility and practicality of electrochemical conversion methods, as it eliminates the need for extreme conditions (such as high temperatures or pressures) that may be associated with other technologies. Furthermore, the high controllability of electrochemical processes is a significant advantage. The precision and fine-tuning afforded make it particularly advantageous for practical applications and hold considerable promise for industrial prospects. The ability to manipulate and regulate electrochemical reactions allows for tailored parameter, optimizing reaction conditions and product selectivity.

1.2.2 Foundation of Electrochemical CO₂RR

The electrochemical reduction of CO₂ entails transforming CO₂ into chemical products through the application of electrical energy with the presence of electrocatalysts. This process is facilitated by the exchange of electrons between the electrocatalyst, CO₂, and solution components. In the experiments, a traditional H-type cell configuration is always utilized, where the working electrode and reference electrode are placed in the cathode chamber while the counter electrode is in the anode chamber opposite to it. All electrodes are immersed in an electrolyte capable of dissociating ions to facilitate charge transfer (Generally, 0.5 M KHCO₃ aqueous solution is chosen as the electrolyte). The cathode and anode chambers are connected through a channel, separated by a membrane [25]. To ensure saturation of the electrolyte, CO₂ gas will be continuously introduced into the cathode chamber during the reaction. Gaseous products generated during the reaction are directed into a gas sampling loop for identification and quantification [26]. Typically, CO₂ is

introduced into the electrolyte for at least 30 minutes before the reaction to ensure electrolyte saturation and eliminate residual air. The reduction reaction, leading to the production of reduced products such as carbon monoxide and formic acid, will be initiated by applying an external voltage or current. Liquid product detection can be accomplished using ion chromatography and/or proton nuclear magnetic resonance (NMR). Here, when applying voltage or current in the electrochemical process, complex interactions occur between ions in the electrolyte solution and the electrodes, resulting in different regions: the electrode surface, the inner Helmholtz plane, the outer Helmholtz plane, the diffusion layer, and the bulk solution. Each region plays a crucial role in shaping the electrochemical environment. Recent report indicates that the surface charges play a vital role in enhancing the selectivity of the CO₂RR [20].

In principle, the electrochemical generation of formic acid from CO₂ occurs at an electrochemical potential of approximately -0.250 V vs. RHE (Reversible Hydrogen Electrode) at pH 7. However, practical considerations necessitate a more negative overpotential because of the intricate mechanisms and slow kinetics involved. The overpotential in the hydrogen evolution reaction (HER) falls within the potential range that competes with CO₂ conversion. The competition of HER poses a significant obstacle to achieving high selectivity for electroreduction of CO₂ to carbon-based products.

Consequently, ongoing research predominantly concentrates on developing electrocatalysts with heightened activity and selectivity. These catalysts aim to expedite reaction kinetics and enhance efficiency by lowering the reduction potential required. The primary objective is to tackle the challenges posed by intricate reaction pathways and slow kinetics, particularly during the formation of the CO₂ radical intermediate. By designing catalysts that facilitate more efficient electron transfer and reduce the overpotential necessary for formic acid generation, researchers seek to improve the overall performance of CO₂ electrochemical reduction. It is essential to note that the detailed mechanism of CO₂ electrochemical reduction to formic acid remains incompletely understood [20].

The CO₂RR process on the surface of electrocatalysts undergoes the following distinguishable stages: CO₂ adsorption and surface interaction, CO₂ activation and reduction, and product desorption and catalyst recovery. Initially, CO₂ molecules adhere to the catalyst surface and engage in interactions with the catalyst's constituent atoms, establishing the groundwork for subsequent reactions. The activated CO₂ undergoes reduction through catalyst-initiated electron and proton transfers, a pivotal step influencing the overall process efficiency. Finally, the newly formed products detach from the catalyst surface, liberating it for the next cycle of reactions. The elucidation of the mechanism involves a combination of computational analysis, electrokinetic, and in-situ spectroscopic examination. Computational analysis entails assessing the performance of catalysts and their interaction with CO₂, relying on thermodynamic principles. While providing valuable insights into the reaction mechanism and catalyst performance, it is important not to rely solely on computational findings for optimal catalyst selection. Taking reaction kinetics into account is essential for comprehending and optimizing reduction processes. As previously mentioned, the electrochemical reduction of CO₂ is inherently intricate, encompassing multiple electron and proton transfer processes. Thus, the examination of reaction kinetics plays a pivotal role in elucidating factors that influence reaction kinetics, identifying crucial intermediates, and understanding electrochemical activation barriers. Techniques such as kinetic studies, involving Tafel plots, and in situ spectroscopic analysis represent primary approaches.

In the domain of electrochemical CO₂RR carried out in aqueous solutions, complex electron and proton transfer processes are involved, facilitating the conversion to various chemical products. Table 1.2 provides a comprehensive summary of the half electrochemical thermodynamic reactions associated with the principal C1 and C2 products achievable through CO₂RR, along with their corresponding standard redox potentials [27].

Table 1.2 The standard redox potentials for the conversion of CO₂ to various C1 and C2 products in aqueous solutions at standard conditions (1.0 atm and 25 °C).

Half electrochemical thermodynamic reactions	Standard potentials (V vs. SHE)
$\text{CO}_2(\text{g})+4\text{H}^++4\text{e}^-=\text{C}(\text{s})+2\text{H}_2\text{O}(\text{l})$	0.210
$\text{CO}_2(\text{g})+2\text{H}_2\text{O}(\text{l})+4\text{e}^-=\text{C}(\text{s})+4\text{OH}^-(\text{l})$	-0.627
$\text{CO}_2(\text{g})+2\text{H}^++2\text{e}^-=\text{HCOOH}(\text{l})$	-0.250
$\text{CO}_2(\text{g})+2\text{H}_2\text{O}(\text{l})+2\text{e}^-=\text{HCOO}^-(\text{aq})+\text{OH}^-$	-1.078
$\text{CO}_2(\text{g})+2\text{H}^++2\text{e}^-=\text{CO}(\text{g})+\text{H}_2\text{O}(\text{l})$	-0.106
$\text{CO}_2(\text{g})+2\text{H}_2\text{O}(\text{l})+2\text{e}^-=\text{CO}(\text{g})+2\text{OH}^-$	-0.934
$\text{CO}_2(\text{g})+4\text{H}^++4\text{e}^-=\text{CH}_2\text{O}(\text{l})+\text{H}_2\text{O}(\text{l})$	-0.070
$\text{CO}_2(\text{g})+3\text{H}_2\text{O}(\text{l})+4\text{e}^-=\text{CH}_2\text{O}(\text{l})+4\text{OH}^-$	-0.898
$\text{CO}_2(\text{g})+6\text{H}^++6\text{e}^-=\text{CH}_3\text{OH}(\text{l})+\text{H}_2\text{O}(\text{l})$	0.016
$\text{CO}_2(\text{g})+5\text{H}_2\text{O}(\text{l})+6\text{e}^-=\text{CH}_3\text{OH}(\text{l})+6\text{OH}^-$	-0.812
$\text{CO}_2(\text{g})+8\text{H}^++8\text{e}^-=\text{CH}_4(\text{g})+2\text{H}_2\text{O}(\text{l})$	0.169
$\text{CO}_2(\text{g})+6\text{H}_2\text{O}(\text{l})+8\text{e}^-=\text{CH}_4(\text{g})+8\text{OH}^-$	-0.659
$2\text{CO}_2(\text{g})+2\text{H}^++2\text{e}^-=\text{H}_2\text{C}_2\text{O}_4(\text{aq})$	-0.500
$2\text{CO}_2(\text{g})+2\text{e}^-=\text{C}_2\text{O}_4^{2-}(\text{aq})$	-0.590
$2\text{CO}_2(\text{g})+12\text{H}^++12\text{e}^-=\text{CH}_2\text{CH}_2(\text{g})+4\text{H}_2\text{O}(\text{l})$	0.064
$2\text{CO}_2(\text{g})+8\text{H}_2\text{O}(\text{l})+12\text{e}^-=\text{CH}_2\text{CH}_2(\text{g})+12\text{OH}^-$	-0.764
$2\text{CO}_2(\text{g})+12\text{H}^++12\text{e}^-=\text{CH}_3\text{CH}_2\text{OH}(\text{l})+3\text{H}_2\text{O}(\text{l})$	0.084
$2\text{CO}_2(\text{g})+9\text{H}_2\text{O}(\text{l})+12\text{e}^-=\text{CH}_3\text{CH}_2\text{OH}(\text{l})+12\text{OH}^-$	-0.744

1.2.3 Mechanism of CO₂RR to Formic Acid

Formic acid is widely utilized across various industries, including agriculture, pharmaceuticals, the chemical industry, food technology, and natural rubber production [28]. Additionally, formic acid demonstrates considerable promise as a hydrogen storage medium, presenting a notable advantage over gaseous H₂ storage [29]. This quality positions formic acid as a practical and effective solution for H₂ storage, a pivotal element in advancing hydrogen-based energy systems.

Beyond its role as a storage medium, formic acid exhibits versatility as it can be directly employed as molecular H₂ or function as a reactant in various chemical processes without the need for conversion into molecular H₂. Examples include its participation in the hydrogenation of olefins, glycerol, and the conversion of hemicellulose sugar [30], enhancing its applicability in diverse industrial contexts. However, despite these advantageous properties, the use of formic acid as a fuel faces constraints due to its relatively low energy density [28]. This limitation drives exploration into alternative energy carriers with higher energy content for specific applications.

The industrial synthesis of formic acid typically involves processes such as methyl formate hydrolysis, hydrocarbon oxidation, formide hydrolysis, and alkali formates acidolysis. While these methods have been conventionally employed, they are not without challenges. The existing commercial routes often entail complexity, environmental concerns, and reliance on fossil fuels. Additionally, they may encounter issues such as slow reaction rates, the formation of undesirable by-products, and high capital costs and energy requirements, particularly in the separation stage. Ongoing efforts in research and development are concentrated on identifying more sustainable and efficient methods for formic acid synthesis, aiming to overcome these limitations and facilitate the widespread adoption of formic acid as a versatile and environmentally friendly chemical carrier and hydrogen storage medium [31,32]. Alternatively, Formic acid is a product obtained through the electrochemical reduction of CO₂, and it is noteworthy for its significant economic value. As of now, the precise pathway for CO₂RR is not fully established. However, Various researches suggest that the conversion of CO₂ to formic acid can occur through four potential pathways [20], as illustrated in Fig. 1.1.

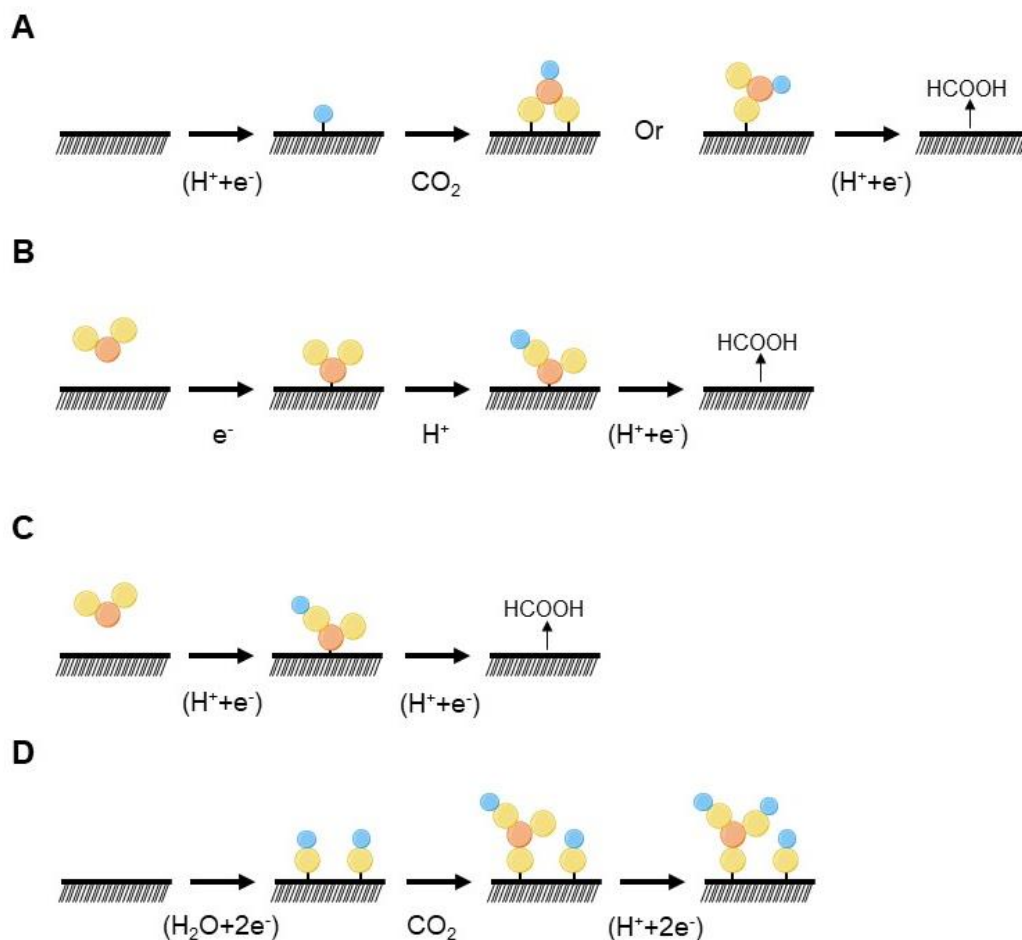


Fig. 1.1 Possible mechanisms to produce formic acid. (A) monodentate intermediate route, (B and C) CO_2 radical anion intermediate route, and (D) surface-bound carbonate intermediate route (yellow ball: O; blue ball: H; orange ball: C).

In the pathway of Fig. 1.1A, an intermediate is generated, attaching to the metal electrode via one or two oxygen atoms. Preceding this stage, the metal electrode forms a bond with hydrogen atoms through direct protonation with H^+ from the solution. This mechanism involves the direct interaction of the metal electrode with hydrogen and oxygen species, leading to the potential production of formic acid. Another possible mechanism (Fig. 1.1B) involves the formation of carbon-metal bonds with carbon derived from the CO_2 radical anion ($\text{CO}_2^{\bullet-}$). In this process, $\text{CO}_2^{\bullet-}$ undergoes reduction by protonating oxygen atoms, resulting in the formation of an intermediate that undergoes further reduction to generate formic acid. It is noted that this mechanism may also

yield carbon monoxide as by-product. This pathway of Fig. 1.1C is similar to Fig. 1.1B but involves COOH directly attaching to the metal electrode instead of forming a $\text{CO}_2^{\bullet-}$. The direct interaction with COOH leads to the subsequent reduction to form formic acid. For example, this specific mechanism takes place at a tin oxide (SnO_2) electrode. In this process, SnO_2 undergoes reduction through a two-electron transfer process to generate Sn oxyhydroxide. The intermediate Sn oxyhydroxide combines with CO_2 to create a surface-bound carbonate, and additional proton and electron transfers contribute to the formation of formic acid.

1.2.4 Electrolyte of electrochemical CO_2RR

The electrolyte plays a crucial role in facilitating charge transfer between the electrode and the catalyst. In CO_2RR , typically, an aqueous electrolyte composed of salts dissolved in a solvent (usually water) is employed. The electrolyte usually consists of cations and either buffer anions or non-buffering anions. In the field of CO_2RR to formic acid, KHCO_3 has become a commonly used and recognized electrolyte due to its high performance [33]. Wu et al. [34] investigated the impacts of different electrolytes (including KHCO_3 , K_2SO_4 , and KCl) on the selectivity and activity of tin-catalysts for formic acid production. The results indicated that KHCO_3 could provide sufficient localized CO_2 dissolution at the interface between electrode and electrolyte, as evidenced by a stable current density over prolonged electrolysis. In contrast, the current densities by using either KCl or K_2SO_4 decreased over time, suggesting the limitations in current density due to the diffusion of dissolved CO_2 . Furthermore, by using KHCO_3 achieved a higher formic acid production rate compared to the cases using KCl and K_2SO_4 , particularly at a potential of -2.0 V vs. SCE. These findings emphasize the importance of electrolyte selection in influencing the performance and selectivity of the CO_2RR process, highlighting the advantages of using KHCO_3 in enhancing stability and formic acid production rate.

1.2.5 Operational Parameters of Electrochemical CO_2RR

Faradaic efficiency (FE) of formic acid and current density is impacted by the flow rate. The effect of flow rate on FE is not particularly notable below 300 mA cm^{-2} . However, beyond 300 mA cm^{-2} , the influence of the CO_2 flow rate becomes notably significant in shaping the FE of formic

acid. Typically, there is a discernible trend of increasing FE with a corresponding elevation in the CO₂ flow rate, reaching an optimal limit. The observation that no further enhancement in FE of formic acid can be achieved beyond the optimal flow rate is indicative of a limiting factor. This limitation is attributed to the constraint imposed by the mass transfer rate of CO₂ in the gas diffusion layer, affecting the transportation of CO₂ to the active site. This implies that at higher current densities, the rate at which CO₂ is delivered to the electrochemical reaction assumes a more crucial role in determining the FE of formic acid production [35]. Meanwhile, the role of the proximate CO₂ concentration near the electrode is pivotal in influencing the performance of an H-type cell. A heightened local CO₂ concentration at the interface of electrode and electrolyte enhances kinetics, leading to improved cell performance. Various factors influence the local CO₂ concentration, such as catalysts, pore structure and the thickness of the catalyst layer [36].

Explorations of electrochemical CO₂RR to formic acid commonly concentrate on ambient temperature and pressure conditions, with limited exploration at higher temperatures. Operating temperature, in general, exerts a notable influence on the electrochemical process since the increased temperature could enhance CO₂ diffusivity and kinetics. However, elevated temperatures also bring about the reduced CO₂ solubility in the electrolyte, affecting the local concentration at the electrode/electrolyte interface and consequently diminishing cell performance. This highlights the substantial reliance of the local CO₂ concentration at the electrode/electrolyte interface on CO₂ solubility.

In the electrochemical CO₂RR, the applied voltage, or current plays a direct role in shaping the product distribution within the cell. Variation in applied voltage could lead to the generation of diverse products, including hydrogen, carbon monoxide, and formic acid. When employing efficient catalysts for formic acid production, the change in applied current could result in the shift in the distribution of formic acid and hydrogen. In general, the primary products are formic acid and hydrogen at low overpotentials. The FE for formic acid production could reach its optimal value as the overpotential increases, accompanied by a decrease in the FE for hydrogen. However, with the further increase in overpotential, the FE for formic acid decreases, and HER becomes dominant.

Consequently, fine-tuning the applied potential or current is essential for optimizing formic acid electrosynthesis [37].

1.3 Electrocatalysts for CO₂RR to Formic Acid

The crucial aspect in the electrochemical CO₂RR to produce formic acid lies in designing and modifying cathode catalytic materials that incorporate a variety of nanomaterial types and classes. Originally, some transition metal catalysts were used in the fundamental research of CO₂RR. Based on the findings, In (Indium), Pb (lead), and Sn (Tin) base catalysts always exhibit a notable preference for producing formic acid. In comparison, Pt (Platinum) and Ni (Nickel) based catalysts always exhibit low activity in CO₂RR, displaying a preference for generating H₂ products. Studt group [28] utilized density functional theory to investigate various metal catalysts and suggested material prerequisites based on thermodynamics. The computations exposed the difficulty in selectively producing HCOOH through the *COOH intermediates reaction pathway, attributed to the strong linear correlation between the chemical adsorption of intermediates and hydrogen adsorption. Additionally, Ag and Pb metals were recognized for having the lowest potential to produce HCOOH and being closest to the minimal thermodynamic potential required for its generation. Nevertheless, the prohibitively high cost of precious metals makes them impractical for large-scale CO₂RR. Bi metal also displays a robust binding affinity with intermediates. Consequently, Pb, Sn, Cu, In, and Bi are acknowledged as electrocatalysts for the CO₂RR to formic acid [39]. Herein, we will primarily introduce those catalysts related to indium, lead, tin, copper, and bismuth for the electrochemical CO₂RR to formic acid.

1.3.1 Bi-based catalysts

Bismuth (Bi) has emerged as a promising metal and a focal point of current research because of its low toxicity and environmentally friendly properties. The initial report on the use of Bi for the electrochemical CO₂RR to formic acid can be traced back to 1995. Hara et al. [40] achieved a high $FE_{\text{formic acid}}$ of 82.7% at -0.72 V (vs. RHE) using Bi in 0.1 M KHCO₃ under a high pressure of CO₂. Also, Bi was predominantly utilized in aprotic electrolyte solutions or ionic liquids for CO

production in the context of CO₂RR research before 2016 [41]. Recently, various reports have been uncovering and systematically evaluating the substantial potential and prospects of Bi-based catalysts for selectively of formic acid. The pre-catalyst method plays a pivotal role in the synthesis of Bi-based catalysts for the CO₂RR. A study by Yang et al. [42] highlighted the preparation of mesoporous bismuth nanosheets through the conversion of bismuth oxycarbonate nanosheets. These nanosheets exhibited a large active surface area and retained the structural integrity. The ultrathin nanosheets demonstrated effective and robust CO₂RR performance, achieving a significant current density of approximately 18 mA cm⁻², excellent FE of nearly 100% at -1.1 V vs. RHE in 0.5 M NaHCO₃, and remarkable operational stability. Furthermore, Gong et al. [43] developed a Bismuth oxide double-walled nanotube catalyst (Bi₂O₃ NTs), where the outer walls are coated with highly defective fragments or clusters. This unique feature was achieved through the selective redox etching of nanotubes. Bi₂O₃ NTs, serving as a template with lattice defects, demonstrated excellent catalytic performance in H-cell testing with high selectivity, substantial current density, and prolonged stability. The distinctive nanostructure of the Bi catalyst played a crucial role in enhancing its activity, confirming its advantage for catalyzing the produce formic acid from CO₂RR.

Introducing other metals into Bi based catalysts can create synergistic effects to adjust the performance and morphology. Zhang et al. [44] proposed a porous catalyst scheme involving the introduction of Cu atoms into bismuth oxide. In their approach, a precursor solution containing Bi³⁺ and Cu²⁺ was mixed with NaNH₄, followed by freeze-drying to obtain the copper-decorated nanofoam catalyst. Subsequently obtained XRD patterns revealed a decrease in diffraction peak intensities with an increasing Cu fraction, indicating that Cu reduced crystallization degree of Bi crystals. Additionally, XPS analysis results showed that presence of Cu changed binding energy. As a result, the catalyst with Cu doping exhibited a maximum current density for formic acid production approximately twice that of the group without Cu. The Cu content was identified as a key factor in regulating electrocatalytic performance and catalyst morphology. Wu et al. [45] introduced a Bi-Sn metal-based aerogel catalyst with a large surface area, achieving a high current density and FE for formic acid production in electrochemical tests.

1.3.2 In-based catalysts

According to the report by Hori et al. [46], In has a promising potential as a metal catalyst for electrochemical CO₂RR to formic acid with a high selectivity (nearly 95%). Leveraging the advantageous properties of In metal, the concept of using In in combination with other metals to form an alloy as a catalyst was proposed by Lai et al. [47]. Experimental findings indicated that the addition of Sn to the In crystal phase can significantly enhance catalytic activity. The highest selectivity of formic acid was achieved when the In and Sn content in the alloy is 90% and 10%, respectively. Importantly, the In_{0.9}Sn_{0.1} electrode maintained a relatively high current efficiency even after a lengthy electrolytic operation of 22 hours. Here, the incorporation of In with Sn can reduce the size of the catalyst, thereby providing more catalytic activity sites. Moreover, the main superiority over conventional Sn metal catalyst lies in their enhanced catalyst stability over an extended period. Meanwhile, the unique crystal phase structure of In-Sn alloy contributes to its remarkable reducibility and durability. In addition, XRD analysis revealed an offset diffraction peak in the In_{0.9}Sn_{0.1} alloy sample and alloying with Sn induced anomalous structural evolution in In, resulting in a face-centered structure dominated by the β phase compression, and this evolution increased the hybridization of 5s and 5p valence electron bands, ultimately enhancing its reducibility and durability.

In recent years, several initiatives have been proposed focusing on the development of single-atom electrocatalysts to produce formic acid. Lu et al. [48] presented a scheme involving atomically dispersed In metal on an N-doped carbon skeleton (In-N-C). In this approach, In atoms were initially incorporated in ZIF-8 to create a precursor. Here, employing a procedure reminiscent of a metal replacement reaction, indium (In) atoms took the place of zinc (Zn) atoms in the dodecahedral coordination center of ZIF-8, and the establishment of the atomic dispersion structure featuring indium In atoms is a noteworthy aspect of this study. Through the utilization of a coordination bond formation process, the coordination bonds between In and the surrounding N and C atoms were forged. This approach, in contrast to directly introducing In atoms into the center of ZIF-8, significantly boosted the interaction force between In atoms and the non-metallic support.

Consequently, the subsequent HAADF-STEM characterization revealed no agglomeration of atomically dispersed In species, and electrochemical testing demonstrated that the FE reached up to 80% at a high current density.

1.3.3 Sn-based catalysts

Sn-based catalysts receive widespread attention due to the low toxicity, abundant availability, and cost-effectiveness. Castillo et al. [49] investigated the electrochemical CO₂RR to HCOO⁻ using a gas diffusion electrode (GDE) with Sn catalyst. They observed a significant impact of Sn loading on the selectivity and current density. Subsequent evaluations focused on the effects of particle size and Sn loading amount for continuous produce products. The optimal performance was achieved with Sn particle size of approximately 150 nm. Moreover, the electrode with a lower amount of Sn loading demonstrated greater efficiency for HCOO⁻ production compared to the case with a higher loading [50]. In a separate study, Yadav et al. [51] showcased HCOOH production over the similar Sn-based catalysts, achieving a maximum FE in KHCO₃ electrolyte.

Despite the high selectivity of Sn-based catalysts for formic acid, they still face challenges such as a narrow potential window and low electrochemical stability. Tsujiguchi et al. [52] discovered that the synergistic effect of Sn/reduced graphene oxide (rGO) composites can significantly enhance the FE. After treating at a high temperature, it exhibited the highest CO₂ adsorption capacity, much higher than the catalysts without addition of rGO. Meanwhile, incorporating metallic heteroatoms into Sn can enlarge electron transfer, leading to the formation of high-valence Sn sites with an upshift in the p- and d-bands. It is considered that this configuration is favorable for the adsorption and stabilization of intermediates, which is crucial in the electrochemical CO₂RR[53-56]. In addition, compared to metal dopants, non-metal dopants are expected to exhibit a stronger ability to change the electronic structure of Sn, due to their significantly higher electronegativity [57].

1.3.4 Pb-based catalysts

Lead (Pb) emerges as another catalyst with notable selectivity for formic acid. Koleli et al. and Innocent et al. [58-60] have already documented FEs ranging from 65% to 74% when utilizing Pb

plate and Pb granule electrodes. Nevertheless, the achieved electrolytic current density with these Pb electrodes remains relatively low. Lee et al. [61] demonstrated that the FE could be significantly improved to 98% when utilizing oxide-derived Pb catalysts. Modification was also applied to optimize the formic acid selectivity of Pb-based materials. It is found that the electrode comprised of $\text{Sn}_{56.3}\text{Pb}_{43.7}$ demonstrated the highest catalytic efficiency, achieving a FE of 79.8% with a high current density. Choi et al. [62] conducted a detailed investigation of the properties of the catalysts using the cyclic voltammetric method. Their findings revealed that Sn atoms in the Sn-Pb alloy play a great role in facilitating the formation of SnO_x and elemental Pb. It indicated that the addition of Sn metal can prevent the formation of low-conductivity PbO, thereby improving performance.

1.3.5 Cu-based catalysts

Cu stands out as a high effective electrocatalyst for CO_2RR , demonstrating a notable ability to produce various products at substantial current densities [63]. Li et al. [64] highlighted the excellent FE of Cu particles synthesized from Cu_2O , in electrochemical CO_2RR to CO and formic acid under significantly low overpotentials in 0.5 M NaHCO_3 . Another study exploring the electrochemical behavior of the Cu/CuO electrocatalyst in a potassium-based solution showcased its enhanced CO_2 reduction capability. In addition, diminishing hydrogen evolution can enable a higher proportion of protons to engage in the reaction [65]. The production of multiple products introduces complexity to the process. To address such challenges, it is essential to convert CO_2 into a single product with a high FE. In a distinct experiment focused on electrochemical CO_2RR to HCOOH, Huan et al. [66] accomplished an impressive 90% FE utilizing a Cu complex as an electrocatalyst.

1.4 High-entropy materials

High-entropy materials (HEMs) for electrocatalysis have been attracted rising attention of researchers, which include high-entropy alloy [67], sulfide [68], phosphate [69], oxide [70]. The design strategy of this material always emphasizes that all participant elements are concentrated together with no obvious base element. Take high-entropy alloy as an example, the earliest reference defined it as the alloy consists of 5 or more principal elements with the same amounts. As such, the

same concentrations of the presented elements limit the design and fabrication of HEA. In the following studies, the HEA definition is expanded based on entropy or composition, and the obtained HEAs are not limited to this circumscription. Generally, the configurational entropy of such materials can be calculated by $\Delta S_{mix} = R \sum c_i \ln c_i$. where R is the molar gas constant, and c_i is the mole fraction of the i -th element [71]. As such, based on the entropy magnitude, alloys can be divided as low entropy alloy (LEA, $\Delta S_{mix} < 0.69R$), medium entropy alloy (MEA, $0.69R < \Delta S_{mix} < 1.61R$) and high entropy alloy ($\Delta S_{mix} > 1.61R$). It should be stated that some researchers define the boundary of MEA and HEA as $1.5R$.

For the composition definition of HEA, it is believed that such a material should contain five or more elements and each with 5% ~ 35% atomic concentration [72]. Besides, a simple crystal structure should be formed by those principal elements in HEAs [73]. However, some materials that beyond the above definition are also considered as HEA, for example, those materials by using minor elements to adjust the performance of HEA, which further extend the scope of HEAs [74]. The consisted elements of HEAs involve alkaline earth metals, transition metals, metalloids, basic metals, and even nonmetals, in which Fe, Co, Ni, Cr, Mn, Cu, Hf, Ti, Ta, Mo, V, Nb, Zr, Zn, W, Si, Al, P and B are generally selected as the composition elements in electrocatalysts [75]. With the variety of elements increasing in an alloy crystal, the contribution of mixing entropic can surpass the effect of enthalpic, resulting in a stable solid-state (SS) solution. While, by regulating the structure, constituent elements and proportions, mechanical ductility, strength, fracture toughness, conductivity, and paramagnetism could be enhanced [76].

The nearby atoms of discrepant elements of HEM-based catalysts can form various unique binding sites in electrocatalysis, leading to almost continuous distribution of the associated adsorption energies, which offer the basis for minutely adjusting the binding energies and finally modulate reaction steps to enhance the reaction kinetics and rate. Herein, the components and structure of the HEM play crucial role in building the system of multiple active sites [77]. By regulating the composition and configuration of multiple elements in HEMs could maximize the synergy effect among various active sites and finely adjust the electronic structure, thereby

enhancing the intrinsic activity of the catalyst and reducing the energy barrier in the electrolysis process.

1.4.1 Structural features of HEMs

To date, various high-entropy electrocatalysts with different phases have been synthesized for electrolysis, in which how to obtain a stable phase is prerequisite question. Generally, the phase of HEA can be evaluated by the mixing enthalpy, mixing entropy, electronegativity, atomic size and valence electron concentration (VEC) [78]. Among them, the entropy plays an important role for forming a single-phase SS, whereas Gibbs free energy difference (ΔG) and atomic size difference determine the formation of a stable phase. Herein, the Gibbs free energy difference depends on the values of temperature, mixing enthalpy (ΔH_{mix}) and mixing entropy (ΔS_{mix}) as expressed in eq.: $\Delta G_{mix} = \Delta H_{mix} - T\Delta S_{mix}$. While, the VEC and electronegativity difference influence the phase transformation and structural stacking property of HEAs. Almost all the HEAs can be synthesized and tuned by controlling these factors. As introduced above, the multiple elements in the HEA can build a simple crystal structure, including intermetallic (IM) compound phase, solid solution phase, amorphous (AM, noncrystalline, glassy) phase and their mixture. In this case, a word of “solid solution” is usually used to describe a family of materials which have a range of compositions and a single crystal structure, in which the solute elements are totally compatible with solvent atoms [78].

It was verified that the participant elements to form FCC and BCC solid solutions in HEA should be carefully selected, in other words, not all the alloys with five-principal elements can form HEA solid solutions. Since there is not a phase diagram on more than quaternary systems, most of the HEA SS are confirmed by a trial-and-error process [79]. However, refer to the Hume-Rothery rules for fabricating conventional alloy solid solution, researchers have proposed some parameters to predict the phase formation of HEAs. While, maybe due to the complex structure and multiple elements, this rule is not always applicable to fabricate HEA solid solution [80]. For instance, it cannot explain the formation of FCC-typed alloy solid solution with equiatomic Co(hcp)-Cr(bcc)-

Cu(fcc)-Fe(bcc)-Ni(fcc), and the conversion mechanism of FCC-type CoCrCuFeNi to a BCC structure by addition of FCC-Al [81].

In addition, some researchers notice the influence of chemical order on the performance of electrocatalysts. And the short-range order (SRO) in nanostructured HEM could accompany with rich grain boundary, defect structure and additional active sites. Besides, it was reported that the large interlayer spacing of short-range ordered structure in the amorphous materials can accept more ions and tolerate volume expansion. It was found that there are a number of small units with lot of disorderly atoms in the short-range-order, which is more adaptable and flexible to tolerate the volume expansion during reaction [82].

Furthermore, amorphous HEAs without a crystal structure are also widely studied for electrolysis. Herein, for amorphous HEA, the glass-forming ability (or amorphous structure-forming ability) can be greatly enhanced by applicable addition of more elements. As reported by the Zhang group [83], there are two types of elements in alloys. The type-I elements are the discrepant elements in the heat of mixing and atomic size, which are generally recognized to have high glass-forming ability in alloy. While, the type-II elements have similar property and are close to each other in the periodic table. The type-I elements can improve the glass-forming ability by improving the viscosity and atomic packing efficiency of alloys. While, the type-II elements can also increase the glass-forming ability due to the high-entropy effects of HEA [80]. Compared with the crystalline HEAs, the amorphous ones could reveal better electrocatalytic property due to its unusual atom arrangement. In general, the amorphous HEAs have rich defect structure (e.g., free-volume zones), loosely bonded atoms, rich coordinatively unsaturated sites, and high corrosion resistance [84].

1.4.2 Four core effects

Stimulated by the unusual performances of HEMs, researchers devote lots of efforts to revealing the enhancement mechanism. Among various HEMs, the effect of entropy change on HEA performance has been most broadly and deeply studied, in which four “core effects” have

been proposed: high-entropy effect, sluggish diffusion effect, lattice distortion effect, and cocktail effect.

The multi-elements in HEMs result in high configurational entropy and lead to a low Gibbs free energy, which overcomes the miscibility barrier. This phenomenon is known as high entropy effect. The mutual solubility among various elements leads to reduced number of phases in HEA. Some studies have shown that single-phase HEAs exhibit superior electrocatalytic performance compared to multiphase HEAs [77]. For example, Bi et al. reported that the NiFeMoCoCr HEA with single FCC phase showed higher HER activity than that one with FCC+ μ dual-phase. They speculated that the better electrocatalytic properties derived from the good electric conductivity, the atoms disorder structure and simple phase. Besides, the surface of FCC HEAs was believed to have more coordinative atoms than the one with dual phase due to the relatively high atoms disorder, which could facilitate the interaction of the electrode with reactant [77]. High entropy effect is one of the four core effects of HEMs along with the lattice distortion effect, sluggish diffusion, and 'cocktail' effect.

The lattice distortion effect is attributed to the asymmetric bonding structures and electron distributions caused by the different atomic sizes of elements. When the atoms are randomly distributed in the lattice, lattice distortion arising from significant atomic size mismatches results in HEMs being in a thermodynamically non-equilibrium state which may lower the energy barriers for molecule adsorption, activation, and conversion in electrocatalytic reactions [85]. Huang et al. showed that lattice distortion can control the displacement of atoms on the surface of nanoparticles, thus improving catalytic performance [86]. The sluggish diffusion effect of HEMs refers to the slower phase transformation and diffusion kinetics compared to conventional alloys. This can be attributed to two main factors. Firstly, the fluctuation of lattice potential energy between lattice sites is significant, leading to slow diffusion rates and high activation energies. Secondly, different atoms exhibit distinct diffusion behaviors. Phase transformations generally require the collective interaction of all atoms, and in particular, grain growth necessitates the migration of all elements together. The slow diffusion can decelerate the rate of grain growth and reduce grain coarseness.

The sluggish diffusion effect in the preparation of HEMs can be utilized to control the microstructure of catalysts. Moreover, the reconstruction of phases also requires the collective diffusion and redistribution of all elements. This phenomenon is advantageous in maintaining the long-term stability of catalysts [87]. The term of "cocktail effect" was first used by Professor S. Ranganathan and refers to this phrase where the properties of a material are determined by the synergistic interaction of its constituent components rather than being a simple linear combination of the effect of each component [88]. It can be considered a complex phenomenon influenced by high entropy, lattice distortion, and sluggish diffusion effects. It reminds us to maintain an open-minded attitude towards non-linear and unexpected results, which may arise from the combination of various constituent elements and microstructures.

In conclusion, the four core effects of HEMs influence the binding sites, electronic cloud distribution, and crystal structure, leading to enhanced catalytic performances compared to traditional catalysts.

1.4.3 Synthesis of HEMs

The synthesis of HEMs is much more difficult than that of traditional materials with unitary compound. At the beginning, the bulk HEAs were generally manufactured by the casting and melt spinning methods [89]. Subsequently, various liquid-state synthesis methods such as the casting, melt spinning, and arc-melting methods [90], zone melting, selective electron beam melting [91] and laser cladding methods [92] were developed to manufacture the bulk HEAs. Herein, the casting and arc melting are conventional ways to produce HEA. For the arc-melting, the alloying raw materials are heated up to a temperature above the melting points of its elements to form a mixed liquid, which is then solidified and heated. The main challenge of this method is the discrepancy in melting points and vapor pressures of the different alloying elements at high temperatures. Besides, the direct laser melting to manufacture the bulk HEAs was also reported, [91] by which the elemental distribution is more homogeneous than that by the as-casted sample [93]. Metal additive manufacturing is an emerging method to produce bulk HEAs, which is a layer-wise fabrication process. During the fabrication process, the metal atoms are bonded together by melting and

sintering processes with high energy sources such as electron beam, high power laser and plasma arc [94]. Compared to the traditional fabrication routes, the metal additive manufacturing endows the advantages of wide component choice, wide structure design freedom and high material usage efficiency [95].

The bulk HEAs with a smooth plane have only a few structure defects with a good mechanical strength. However, the electro-catalysts are expected to have large number of active sites, which is limited by the smooth plane of bulk HEAs. Hence, changing such planar bulk materials into the nanostructured ones can greatly improve the amount of exposed active sites. To date, some synthetic routes for the fabrication of nanostructured HEAs have been proposed, by which it is expected to obtain nanoparticles with controllable multi-elemental composition with suitable particle size as well as morphology and little contamination.

There are two main tactics to design nanostructured HEAs, i.e., top-down and bottom-up routes. The typical routes of the first one contain crush the bulk materials to nanoscale debris by employing additional energy sources such as mechanical, thermal, chemical and laser irradiation methods. Especially, the mechanical alloying, dealloying, laser ablation and photolithography are some of the commonly used top-down approaches to prepare HEA.

The mechanical alloying, such as high-energy ball milling, is a powder metallurgical technique, which includes the processes of repeated cold welding, fracturing, and re-welding of blended powder. This method can motivate the mechanical activation and/or elicit the chemical reaction of the powder reactants [96], which is an efficient route to manufacture HEA nanoparticles since it can reduce the occurrence of segregation comparing with the thermal melting method. Nellaiappan et al. [97] synthesized AuAgPtPdCu nanoparticles by using a cast cum cryo-milling process, which showed good catalytic activity for electrochemical reduction of CO₂. Xu et al. [98] fabricated the high entropy zeolitic imidazolate framework (HE-ZIF) via a methodology of vigorous ball milling, which also showed high catalytic activity for CO₂ fixation due to the synergistic effect of the different metal ions as Lewis acids in epoxide activation. Besides, an

efficient method to modify the surface of HEA is laser ablation, which can remove lots of species from the solid by applying short-intense-laser pulses on the surface. For example, Redka et al. [99] studied the effect of ultrashort-pulse laser-matter interaction on the morphology of CrMnFeCoNi alloy and found that the smooth surface of HEA was ablated to rough gaps. A melting combined dealloying method has also been used to prepare HEA with nanoscale pores [100]. This dealloying route always utilizes different activities of dissolution or diffusion reaction of various elements during the etching process to fabricate a porous material. Especially, those unstable species of HEA will be selectively attacked by the acidic or basic chemicals, dissolving from a multicomponent alloy. The main challenge of this method is controlling the dissolution or reestablishment of various elements to obtain HEM with ideal microstructure and composition. Meanwhile, the casting process of alloy precursors requires inert atmosphere and high temperature [101]. Besides, one should pay attention to avoid the phenomenon of segregation, bulk accumulation etc.

The opposite synthesis strategy of HEM NPs is a bottom-up approach, which is generally conducted by the chemical reactions of various atoms or molecular species. There are some efficient methods such as ionization, sublimation, dissociation, or evaporation of gas or liquid to obtain a precursor, which was further to be converted to crystalline or amorphous nanoparticles [101]. This method provides an efficient route to prepare HEM nanoparticles rapidly and facilely with a controllable shape, size, and composition. Sputter deposition is a kind of physical vapor deposition (PVD), and a popular route to control the HEA morphology, by which the target surface is bombed with gaseous ions to dislodge surface atoms or clusters, following by deposition in a medium (e.g., ionic liquids) to form NPs. This method can separately adjust the elemental sputter targets and the corresponding deposition rates so as to control the composition of HEA material. Furthermore, the nanostructured HEA with a tunable shape and size can be realized by using ionic liquids instead of the solid substrate, in which the ionic liquids act as the stabilizer and suspension medium for NPs formation by conducting low vapor pressures and melting points [102]. The shortcoming of sputter deposition is the requirement of deposition equipment and ultrahigh vacuum. To date, many HEA NP systems have been built rapidly by using the sputter deposition, in which the compositional

variation is large but controllable. Meanwhile, Schuhmann et al. [103] synthesized multinary CrMnFeCoNi alloy by conducting co-sputtering into an ionic liquid, which showed a high catalytic activity toward oxygen reduction. These studies demonstrate the potential of HEA for catalytic application by nanostructuring the morphology and adjusting the composition.

Recently, scanning probe block copolymer lithography has been used to synthesize HEAs, in which the elements of block copolymer lithography are combined with the scanning probe technique. By using this method, the obtained AuAgPdNiCoPt alloys showed nanoparticle morphology with diameters in the range of 10-20 nm [104]. Carbothermal shock (CTS) is also a popular method to prepare nanostructured HEA, which includes rapid heating and cooling of metal precursors on oxygenated carbon supports with controllable shock time as well as ramp rate. Herein, the fast thermal decomposition of precursors at high temperature results in the formation of small droplets of multi-elements liquid, which can be crystallized into homogeneous alloy NPs via subsequent rapid cooling process [105]. The HEAs obtained by this method always have a small size distribution. In this method, the high temperature rapidly drives the particle “fission” and “fusion” events, leading to uniform mixtures of multiple elements. While, the structure and dispersity of particles can be controlled by turning the shock parameters like temperature, duration, and cooling rate. Comparing with the conventional wet impregnation method, the overall chemical and structural stability of the electrocatalyst with the same compositions was greatly enhanced. However, the synthetic process of CTS method is conducted on the suitable substrate (carbon supports), which is hard to ameliorate. And the production of this method is only in milligram scale. And the cost and high requirement of equipment are expected to be reduced in the future.

Another popular route of HEM nanoparticle synthesis is based on wet-chemistry methods, in which adjustable particle size, shape, and phase can be realized. However, the composition of the alloys synthesized by wet-chemical methods generally cannot exceed three elements, which thusly need more substantive theoretical and experimental studies to adjust the structure and composition of HEM. Herein, Hydrothermal and solvothermal processes are two typical wet-chemical synthesis methods [107], which are related to the solubility of the materials under high

temperature and pressure in an airtight container. These approaches are good at regulating the morphology, crystal, and surface chemistry by adjusting the feeding composition, pressure, temperature, additives, solvent, and aging duration. Wet-chemical synthesis followed by pyrolysis is a promising way to manufacture HEMs, in which the precursors are prepared by the wet-chemical route followed by pyrolysis of them to HEMs. Some modified wet-chemical approaches have been applied to synthesize nanostructured HEA. For example, Dai et al. [108] demonstrated the synthesis of PtAuPdRhRu HEA with 3 nm diameter by using ultrasonication assisted wet chemistry method, in which, during the ultrasonication process, the noble metal precursors were reduced together by the chemical reductants, and then converted to alloy due to the acoustic cavitation. As a special wet chemical method, Electrodeposition employs charges as the reductant to deposit alloy. This method can efficiently regulate the performance of obtained HEA since there are many adjustable parameters to control the HEA structure and composition. For example, Wang et al. [109] used ZnO nanorod array template to assist electrochemical deposition of quinary PdNiCoCuFe alloy nanotube, and found that the obtained ZnO@PdNiCoCuFe core-shell composite had good electroactivity and durability for the methanol oxidation. While, due to the multi-layer deposition process, there is obvious stress difference between each layer, which may result in structure defects. Besides, in order to obtain HEM with rational composition, one should pay attention to the discrepant thermodynamics of different ion reduction [110].

1.4.4 Characterization

As stated above, the HEM has randomly mixed multiple elements in one single crystal, whose morphology, crystalline structure; elemental state can be characterized by conventional techniques such as scanning electron microscopy (SEM), transmission electron microscopy (TEM), powder x-ray diffraction (XRD) and x-ray photoelectron spectroscopy (XPS). However, it has a great challenge to distinguish the configuration of mixed atoms. Recently, various synchrotron X-ray based techniques that employed shorter wavelength offer a higher resolution to reveal the atomic bonding, arrangement, and electronic properties of HEM. For instance, synchrotron XRD is good at detecting the phase structure and immiscible phases to notarize the realization of HEM [111]; X-

ray absorption spectroscopy (XAS) can be used to expose the coordination environment of different elements for the understanding of the multiple elemental states and local orders of HEM [112]; and the hard X-ray photoelectron spectroscopy (HAXPES) has been widely employed to analyze the valence band and d-band center of HEMs to study the adsorption energy of key intermediates, thereby helping to explain the catalytic activity [113]. While, four-dimensional scanning transmission electron microscopy (4D-STEM) has become to an important electron microscopy technique to reveal the morphology, crystal, composition, phase and so on [112], by which the local diffraction patterns and corresponding strain maps can be realized via comparing the discrepancy between the average and local phase structures for understanding the exposing of the potential lattice strain and distortion [114]. Recently, atomic electron tomography (AET) has been used to display the 3D atomic structure of an amorphous HEA nanoparticle, including Ni, Co, Rh, Ru, Ag, Pd, Pt and Ir elements [115]. Herein, four kinds of medium-range ordering crystals are presented in the 3D atomic structure, which includes FCC, BCC, hexagonal close packed (HCP), and simple cubic structures. These advanced technologies provide direct observation results for the analysis of the characteristics of nanostructured HEM at the single-atom level [116].

Even though, it is still full of challenges to design and identify the catalytic active sites in HEM due to the complex structure, electron distribution and binding energy distribution. Recently, first-principle-based methods have been employed to study the relationships of structure-composition-property of HEM-based catalysts [117]. Especially, high throughput computation is a powerful method to predict the phase of HEM by following phase diagram calculation or empirical rules, which can screen millions of elemental combinations [118]. It should notice that high-throughput screening mainly focuses on the bulk materials. When it is used to design nanostructured HEM, one may consider building more precise atomic packing models and binding sites due to the influences of small size and nonequilibrium synthesis conditions.

1.5 Anode Reaction: Oxygen Evolution Reaction

In a typical electrochemical CO₂RR system, while the cathode serves for the CO₂RR, the anode provides a site for the oxygen evolution reaction (OER) (Fig. 1.3).

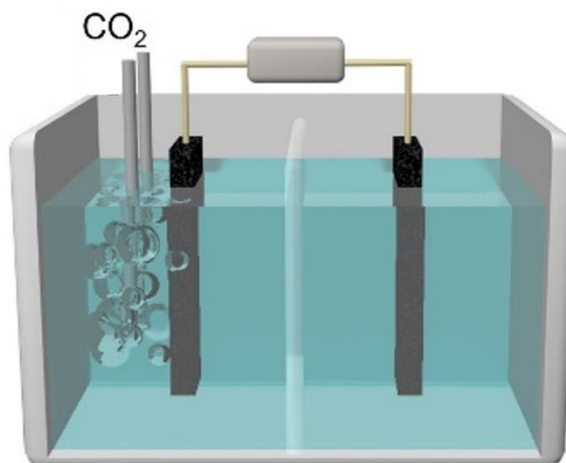


Fig. 1.3 Schematic diagram of an electrolyzer for electrochemical CO₂RR system, in which CO₂RR occurs on the left side while OER on the right side.

As in the seawater electrolysis system, OER also occur in the electrochemical CO₂RR system. Since the electrocatalysts used for OER in the seawater electrolysis system could be also applied in the electrochemical CO₂RR system. In the following, the mechanism of OER and its competition with CER over the electrocatalysts in seawater environment, and especially the application of high-entropy materials in OER will be reviewed.

1.5.1 Fundamental of OER

The OER is a complex 4-electron transformation reaction. (Figures 1.2) It is worth noting that in acidic electrolyte, water is oxidized to form oxygen ions and hydrogen ions, while in basic electrolyte, hydroxide ions are oxidized to form water and oxygen. Regardless of the reaction conditions, there are typically the same intermediates including the HO_{ad}, O_{ad}, and HOO_{ad} [119].

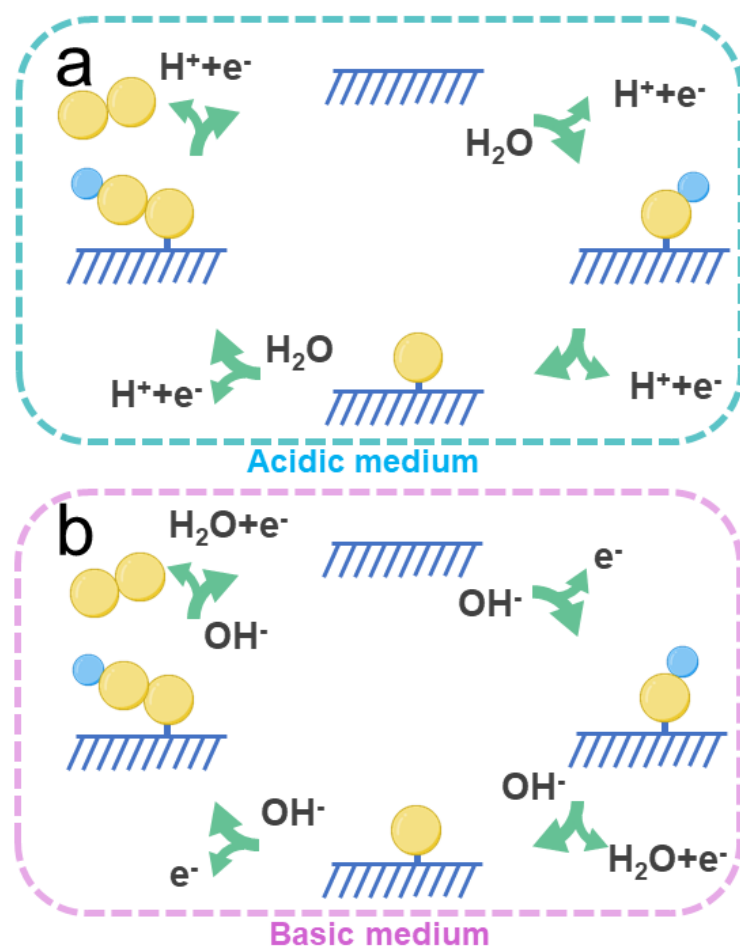


Fig. 1.2 Mechanisms for OER in (a) acidic medium and (b) basic medium (yellow ball: O; blue ball: H).

The thermodynamic equilibrium potentials of OER relative to the reversible hydrogen electrode (RHE) are closely related to the pH value. Under standard conditions (1 atm, 25°C), the theoretical potentials follow the Nernst equation based on the pH value. However, no electrochemical reaction occurs when the applied potential reaches the predicted value in practical systems. The reason is that actual environment is more complex than the theoretical environment, and additional driving forces are required to provide more potential energy to overcome the kinetic and thermodynamic barriers. Overpotential (η) refers to the additional potential input required to drive the reaction relating to the ideal potential. Lower overpotential indicates a lower starting potential for occurrence of reaction. Overpotential for a given current density and Tafel slope are most important parameters used to evaluate the performances of OER. The sources of overpotential mainly include

concentration polarization, ohmic resistance, and activation overpotential. Concentration polarization occurs when the current passing through the electrode/solution interface causes a change in electrolyte concentration. This can result in the decreased electrolyte conductivity or the increased solution resistance when the polarization current is large. Concentration polarization can be reduced by stirring the solution. The voltage drop in the electrolyte can be compensated using the iR compensation method. Activation energy (activation overpotential) reflects the catalytic ability of the electrode material for the reaction and is an inherent property of the electrode material.

1.5.2 Oxygen evolution reaction and chlorine evolution reaction

Compared with freshwater, seawater is the most abundant water source on the planet and accounts for ~96.5% of the total water resource in the world [120]. Therefore, direct seawater electrolysis offers an opportunity for hydrogen production on a large scale [121]. This technology not only alleviates the pressure of scarce freshwater resource to a certain extent, but also shows great practical significance for those arid coastal areas, which tend to have limited freshwater but plenty of seawater and renewable electricity. However, seawater contains high concentrations of Cl^- ions (~0.5 M), and the competing chlorine evolution reaction (CER) on the anode can occur alongside the oxygen evolution reaction (OER) [122]. Additionally, the presence of Cl^- ions can also lead to corrosion of metal electrocatalysts as well as the substrate, significantly reducing their lifespan. In addition, the presence of calcium and magnesium ions in seawater can result in the formation of insoluble precipitates in alkaline environment, potentially covering the catalytic sites and even causing catalyst poisoning [123]. Fortunately, those catalysts with a large surface area and numerous active sites could effectively mitigate these issues.

1.5.3 HEM electrocatalysts for OER

The OER is a complex 4-electron transformation process, including the HO^* , O^* , and HOO^* intermediates in the alkaline solution. Similarly, traditional catalysts cannot meet the requirement of fast adsorption and desorption of various intermediates during the OER [124]. Thus, fine-adjusting of structure and components of HEM-based electrocatalysts to expose efficient multiple catalytic active sites should be a potential route to overcome these challenges. For the HEMs, the

nearby atoms of discrepant elements can form various unique binding sites, leading to almost continuous distribution of associated adsorption energies, thereby providing the basis for the fine-tuning binding energies to modulate reaction properties. Furthermore, in the OER process, HOO^* and HO^* intermediates always interrelate with the catalyst surface via O atoms, and thus optimizing their binding energies could regulate the adsorption behavior of HOO^* and HO^* at different sites and break the correlating scale relationship. Hence, adjusting the composition and structure of HEMs to improve OER performance attracts rising attention [125]. Herein, the synergistic effect of Fe, Co and W elements can lead to an optimized local coordination environment as well as intermediate binding energy [126]. In addition, highly electronegative atoms are good at serving as proton acceptors to stabilize the HOO^* intermediate to yield O-O^* and H^* [127].

Besides, the conversion of surficial species can efficiently adjust the composition of HEM. It was reported that the high applied potential during OER could oxidize the surface of the metal or alloy to form metal oxides or (oxy) hydroxides [128], and the behavior of oxidation of HEAs can be determined by the Kirkendall effect [129], in which the metal elements come out with the formation of an oxidation layer will occur. It should note that the real active species of these HEA catalysts for OER generally are the restructured oxide or (oxy)hydroxide surface layers rather than the original metallic phase. Thus, for the HEM-based electrocatalysts, it should be considered that their structure and components can be further controlled by the rebuilding of superficial species in the OER process, which could reveal stronger synergistic effect with the substrate materials.

Generally, due to the big difference in atomic radius between the constituent metal elements in high entropy oxides, the crystal lattice distortion could easily occur, resulting in the changes in bonds and electron cloud distribution between atoms, which can effectively improve the intrinsic catalytic activity of high entropy oxides [130]. Furthermore, the high entropy oxide is situated at the center of a multivariate phase diagram, which usually has the least exploring area in the material composition to possess unexpected behavior [131].

In this master thesis study, high-entropy compounds for electrochemical CO₂RR as well as for OER in the system were simultaneously developed. It is expected to assemble these two catalysts into an electrolyzer enables a dual-electrode electrolysis reaction for carbon dioxide reduction and water oxidation.

Chapter Two

Experimental Materials and Test Methods

2.1 Experimental Chemicals and Materials

Table 2.1 Chemical reagents used in this study

Chemical reagents	Manufacturer	Purity
Bismuth nitrate pentahydrate	WAKO	99.5%
Copper nitrate trihydrate	WAKO	99.9%
Tin chloride	WAKO	97.0%
Lead nitrate	WAKO	99.5%
Indium nitrate trihydrate	WAKO	97.0%
1,3,5-Benzenetricarboxylic Acid	Tokyo chemical industry	98.0%
N,N-Dimethylformamide, deoxidized	WAKO	99.5%
Methanol	WAKO	99.8%
Cobalt nitrate hexahydrate	WAKO	99.5%
Iron nitrate nonahydrate	WAKO	99.0%
Nickel nitrate hexahydrate	WAKO	98.0%
Manganese nitrate tetrahydrate	WAKO	97.0%
Ammonium fluoride	WAKO	97.0%
Urea	WAKO	99.0%

Table 2.2 Gases used in this study

Reactant gas	Manufacturer	Grade
Argon	TAIYO NIPPON SAN SO	99.9999%
Carbon dioxide	TAIYO NIPPON SAN SO	99.999%

2.2 Experimental equipment

The following is a summary of the instruments and equipment used in the experimental process of this study.

Table 2.3 Experimental Instrument and Equipment

Instrument and equipment	Specifications and models	manufacturer
X-Ray Diffraction (XRD)	SmartLab	Rigaku
Scanning Electron Microscopy (SEM-EDS)	JSM-7000F	JEOL
High-performance liquid chromatography (HPLC)		Shimadzu
Electrochemical Workstation	Versa STAT4	Princeton
Transmission electron microscopy (TEM)	JEM-2100	JEOL

2.3 Characterization methods and testing methods

2.3.1 X-ray Diffraction Analysis (XRD)

X-rays are electromagnetic radiation rays with a short wavelength (0.01~10nm), which can irradiate the material to produce scattering phenomenon. Coherent scattering of X-rays by crystalline materials is a diffraction phenomenon, that is, the incident beam irradiates the material, in which when the outgoing beam does not diverge, its wavelength remains the same, but the direction changes. The phenomenon of X-ray diffraction (XRD) is a phenomenon peculiar to crystalline substances. The characteristic of crystal microstructure is periodic ordered structure, and the X-ray diffraction pattern of crystal is a physical transformation of the 3D scene of crystal microstructure, which contains all the information of crystal structure. Its XRD pattern can be obtained with a small amount of solid powder or a small sample. Thus, XRD stands as the most potent method for examining crystal structures, encompassing details such as the type and distribution of atoms or ions, as well as their groups, along with the shape and size of the unit cell.

2.3.2 Scanning Electron Microscopy (SEM)

In the scanning electron microscope, the electron beam emitted by the electron gun is generally focused by three electromagnetic lenses to form an electron beam with a diameter of 0.02~20 μm . The scanning coil on the upper part of the final lens (also called the objective lens, but it does not magnify and is still a condensing lens) can make the electron beam scan raster on the surface of the sample. Under the action of the electron beam, the sample excites various signals. The intensity of the signal depends on the morphology of the sample surface, the composition of the excited region and the crystal orientation. The high-sensitivity nano-ammeter receives the excited electronic signal, and after the signal processing and amplifying system, it is sent to the grid of the picture tube to modulate the brightness of the picture tube. Since the electron beam in the picture tube and the electron beam in the lens barrel are scanned synchronously, the brightness of each point on the picture tube is modulated by the intensity of the electronic signal excited by each point on the sample, that is, by any point on the sample. The intensity of the collected signal corresponds directly to the brightness of the corresponding point on the picture tube screen. Through the interaction of electrons with substances, diverse physical and chemical properties of the sample can be derived, including morphology, composition, crystal structure, electronic structure, and internal electric or magnetic fields.

2.3.3 X-ray energy dispersive spectroscopy (EDX)

Energy Dispersive X-Ray Spectroscopy, also abbreviated as EDX, is realized by analyzing the wavelength and intensity of element characteristic X-rays emitted by the sample. The SEM-EDX combination is the most widely used microscopic analysis instrument and one of the main means of micro-area composition analysis. EDX has the following characteristics. (1) It can quickly and simultaneously perform qualitative and quantitative analysis of all elements and elements of Be-U in the micro-area of various samples, which can be completed within a few minutes. (2) The requirements for the geometrical position of the sample and the detector are very low and the working distance is not very strict. (3) The probe current required by the energy spectrum is

small so that the damage to the samples that are easily damaged after electron beam irradiation, such as biological samples, fast ion conductor samples, and glass, is small.

2.3.4 Transmission Electron Microscopy (TEM)

TEM is an advanced imaging technique employing a beam of electrons transmitted through a specimen to generate detailed images. Typically, the specimen is an ultrathin section, or a suspension mounted on a grid. The interaction of electrons with the sample as the beam passes through the specimen forms the basis of image formation. In the process, the magnified and focused image is directed onto an imaging device, which may consist of a fluorescent screen, a layer of photographic film, or a detector such as a scintillator connected to a charge-coupled device or a direct electron detector. The high-resolution capability of TEM surpasses those of light microscopes due to the smaller de Broglie wavelength of electrons. This unique property allows TEM to capture minute details, reaching down to the scale of a single column of atoms. To put this into perspective, the resolution achieved by TEM is thousands of times finer than what is attainable with a light microscope. This exceptional resolving power of transmission electron microscopes makes them indispensable in various scientific fields, enabling researchers to delve into the intricate details of nanoscale structures and phenomena.

2.3.5 Electrochemical test

CO₂RR measurements were conducted within a proton exchange membrane (Nafion 117) separated anode and cathode in a standard three-electrode system. The setup included a graphite rod as counter electrode, an Ag/AgCl electrode as the reference electrode, and a CO₂-saturated 0.5 M KHCO₃ aqueous solution (pH=7.21) as the electrolyte. Potentials were converted to the reversible hydrogen electrode (RHE) scale using the formula $E_{RHE} = E_{Ag/AgCl} + 0.0591\text{pH} + 0.225\text{V}$. Linear Sweep Voltammetry (LSV) polarization curves were recorded with a sweeping rate of 10 mV s⁻¹ in the CO₂-saturated 0.5 M KHCO₃.

For the OER activity test, a conventional three-electrode system was employed, consisting of the fabricated electrode as the working electrode, a commercial Hg/HgO electrode as the reference

electrode, and a graphite rod as the counter electrode. The electrolyte used for OER testing was 1 M KOH + seawater solution. Prior to the activity test, the fabricated electrode underwent cyclic voltammetry treatment with a scan rate of 50 mV s^{-1} until a stable CV polarization curve was obtained. The potential ranges for OER and HER activation were $0 \sim 1.5 \text{ V}$ and $-0.5 \sim -1.5 \text{ V}$ (vs Hg/HgO), respectively. The OER and HER activity tests were conducted within the ranges of $0 \sim 1.5 \text{ V}$ and $-0.8 \sim -2.0 \text{ V}$, respectively, with a scan rate of 2 mV s^{-1} . The potential referenced to RHE was calculated as $ERHE = E_{\text{Hg/HgO}} + 0.0591\text{pH} + 0.118 \text{ V}$, and all tested LSV curves were corrected with iR compensation. Chronopotentiometry (CP) was employed to evaluate the stability of high-entropy materials. The electrochemically active surface area (ECSA) of each catalyst was estimated using the double-layer capacitance (C_{dl}).

2.3.6 High-performance liquid chromatography (HPLC)

Liquid chromatography is a method utilized for the separation of a sample into its individual constituents based on their interactions with the mobile and stationary phases. The classification of chromatography types depends on the physical states of these phases, and one widely employed method is liquid-solid column chromatography, which involves a liquid mobile phase filtering down through a solid stationary phase. In this technique, a solvent drip through a column filled with an adsorbent under gravity.

HPLC is an advanced version of column chromatography that operates under high pressures, often reaching up to 400 atmospheres. Unlike column chromatography, where gravity propels the solvent, HPLC employs a pump to force the solvent through the column. The column packing material, or stationary phase, typically consists of granular solid particles like silica or polymers. The increased pressure in HPLC enhances the speed of the process, allowing the use of smaller particles for the column packing material. The smaller particles offer a greater surface area for interactions between the stationary phase and the flowing molecules, resulting in improved separation of mixture components. The pressurized liquid, known as the mobile phase, usually comprises a solvent mixture such as water, acetonitrile, and/or methanol. The diverse interactions of mixture components with the adsorbent particles lead to varying elution rates, facilitating the

separation of components as they exit the column. HPLC, in contrast to column chromatography, is characterized by high automation and exceptional sensitivity.

Chapter Three

Formation of high entropy metal organic frameworks cathode for promoting carbon dioxide reduction reaction to formic acid

3.1 Introduction

High-entropy materials (HEMs) are considered as a new family of electrocatalytic materials. Compared with the bimetallic or ternary metal compounds, HEMs are believed to endow “four core effects”, i.e., high-entropy effect, lattice distortion, sluggish diffusion, and cocktail effect [89]. These usually offer adjustable composition, optimal grain size, stable crystalline structure, modified bond length and good electron cloud distribution, endowing HEMs with long-term stability and unexcepted catalytic performance. Moreover, the complex components and structure of HEMs could result in discrepant atomic distribution and special binding sites, which can modulate the binding energy of reactants in a continuous form by varying elemental ratios. Therefore, compared with those traditional materials, HEMs have highly active sites for adsorption of various reactants and intermediates [113]. Currently, the application of HEMs in CO₂RR is focused on electrochemically reducing CO₂ to CO. For instance, the CO and hydrogen adsorption energies of all surface sites on the (111) surfaces of the disordered HEAs were predicted by Jan Rossmeisl's group[97]. This prediction was achieved through a combination of DFT calculations and supervised machine learning. In addition, Krishanu Biswas manufactured a high-entropy alloy where the carbon monoxide yield reached almost 100% at a low potential of -0.3 V versus RHE [132]. However, the application of high-entropy catalysts in the electrochemical CO₂RR to other products remains unexplored.

Employing high-entropy metal organic framework (HE-MOF) as the self-sacrificial template to fabricate HEMs attracts rising attention. HE-MOF is not only a promising template to obtain nanostructured HEA, but also a good carbon source to fabricate unusual HEM/C composite

electrocatalysts. Besides, catalysts obtained by pyrolysis of MOF precursors can inherit their framework structures with uniform metal sites and high porosity. Especially, the regular confined space formed between carbon materials and metals provides an ideal microenvironment for limiting the size of metal component [133]. Herein, hydrothermal and solvothermal processes are two typical wet-chemical synthesis methods to prepare MOF precursors [134], which are related to the solubility of the materials under high temperature and pressure in an airtight container. Both approaches are good at regulating the morphology, crystal, and surface chemistry by adjusting the feeding composition, pressure, temperature, additives, solvent, and aging duration. However, solvothermal synthesis suffers from low productivity, and the size uniformity of HEAs prepared via this method needs further improvement. For example, Huang et al. used a solvothermal method to deposit quinary MnFeCoNiCu MOF nanorod precursor, which was further pyrolyzed to obtain HEA nanoparticle [86]. Polymetallic MOF precursor is also usable for producing CoNiCuMnAl/C high-entropy composite with a core-carbon shell structure. Herein, the derived carbon in the composite can improve catalytic activity and long-term stability. As such, the obtained composites in this way always show high stability [135].

Herein, a high-entropy metal-organic framework (HE-MOF) composed of Bi, In, Sn, Pb, and Cu was synthesized and deposited on carbon paper (CP) using a hydrothermal method. XRD analysis verified the creation of a high-entropy structure. The catalyst exhibited outstanding performance, featuring high selectivity (exceeding 80% FE) and stability (20 hours) in the electrochemical CO₂RR to formic acid.

3.2 Experimental

The synthesis process involves several steps to treat CP and deposit the high-entropy metal organic framework (HE-MOF) on the substrate.

3.2.1 CP Treatment

The purchased CP was subjected to a treatment process to eliminate impurities, in which the CP piece was immersed in a 3M HCl solution for this purpose. After the treatment, the CP is stored in ethanol.

3.2.2 Precursor Deposition on CP (Hydrothermal Method)

Ingredients: 0.4 mmol $\text{Bi}(\text{NO}_3)_2$, 0.4 mmol $\text{In}(\text{NO}_3)_3$, 0.4 mmol $\text{Pb}(\text{NO}_3)_2$, 0.4 mmol $\text{Cu}(\text{NO}_3)_2$, 0.4 mmol SnCl_2 , 3.5 mmol H_3BTC (1,3,5-Benzenetricarboxylic Acid), 30 mL methanol and 30 mL N,N-Dimethylformamide, deoxidized.

Procedure: Catalysts was deposited on CP by a hydrothermal method, in which a mixed solution of ingredients in the 30 mL distilled water was used and the hydrothermal reaction was conducted at 120 °C and 24 hours. Here, in the Teflon-lined autoclave (100 mL) utilized for hydrothermal synthesis, two pieces of pre-treated CP were used together.

3.3 Results and discussion

3.3.1 Morphology and crystal structure

The fabrication process of BiInSnPbCu-CP involves a hydrothermal process followed by drying at 60°C. After the hydrothermal reaction, as shown in Fig. 3.1, the catalysts are uniformly grown on the CP. From the magnification of the SEM image (Fig. 3.1b), nanospheres with a particle size range of 50-200 nm can be observed.

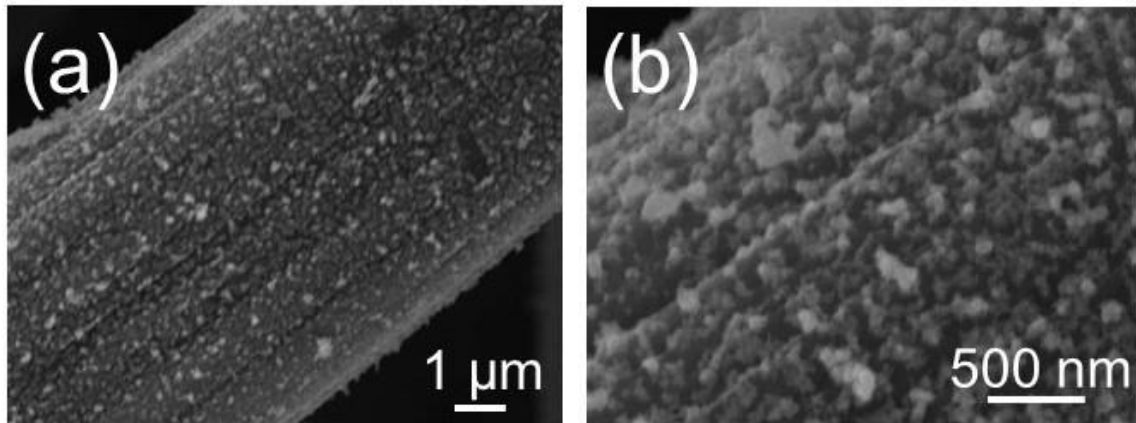


Fig. 3.1 (a-b) SEM images of BiInSnPbCu-CP.

Also, the crystalline structure of BiInSnPbCu-CP was analyzed. As shown in Fig. 3.2, there are four characteristic peaks at 32.5° , 46.7° , 58.1° and 77.7° , which could be attributed to the reflections of the (200), (220), (222) and (420) crystal planes of cubic crystalline of the catalysts (PDF#65-8291, Fig. 3.2). The other two peaks correspond to characteristic features of the CP. Thus, through XRD analysis, we can confirm the formation of a single-phase compound, it is confirmed that the obtained BiInSnPbCu compound should be consistent with the definition of high-entropy materials.

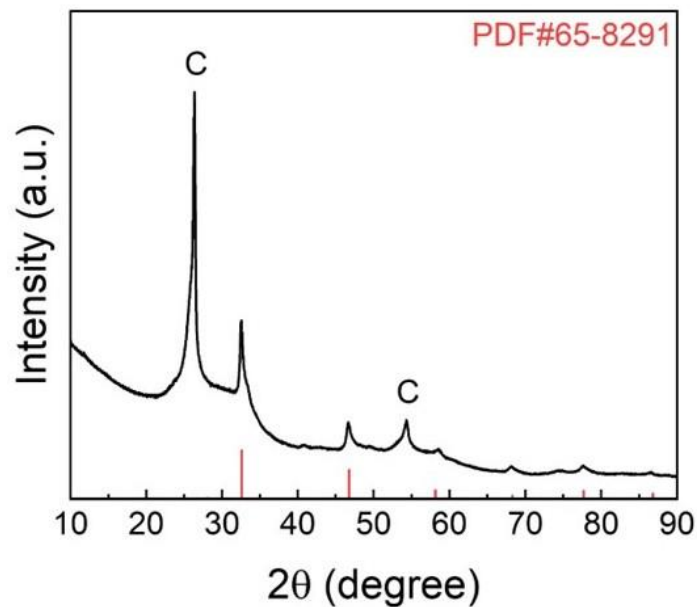


Fig. 3.2 XRD pattern of BiInSnPbCu-CP.

3.3.2 Electrochemical Test

The FE test involves the collection of samples after one hour of continuous potential applying in a 0.5 M KHCO₃ solution saturated with CO₂, which is then analyzed using HPLC to quantify the concentration of the produced formic acid and confirm whether there are other liquid products or not. In this study, the tested applied potential range spans from -0.65 to -1.05 V vs. RHE. As displayed in Fig. 3.3 (a), remarkably, the FE exhibits a special trend. Initially, it increases and then subsequently decreases, and the most favorable applied potential for formic acid production is found to be -0.85 V. At this optimal potential, the corresponding FE reaches as high as 80.7%.

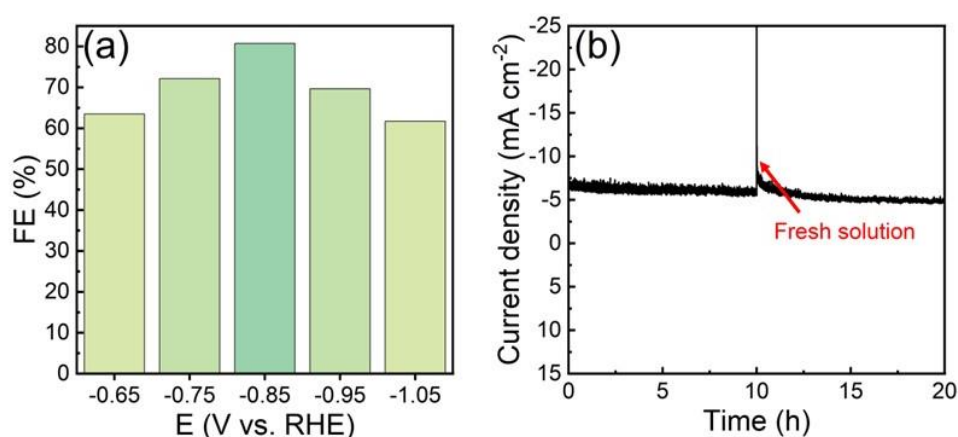


Fig. 3.3 (a) FEs at different applied potentials and (b) i-t test of BiInSnPbCu-CP electrode.

Furthermore, the stability of the electrocatalyst was investigated over an extended testing period. Even after 20-hours of continuous testing, the FE only shows a marginal decrease, declining from the initial 80.7% to 79.4%. This stability is also maintained despite of a reduction in the current from 6.5 to 4.9 mA/cm² over the same period. The minimal decrease in FE suggests that the electrocatalyst demonstrates excellent stability and performance over an extended testing duration.

3.3.3 Conclusion

The synthesis of a HE-MOF electrocatalyst based on Bi, In, Sn, Pb, and Cu grown on CP through a hydrothermal method was performed. The obtained HE-MOF coated cathode denoted as BiInSnPbCu-CP was confirmed through XRD analysis, validating the formation of a high-entropy

framework, which also exhibited exceptional performance in the electrochemical CO₂RR to formic acid, with 80.7% of FE, and even after an extended duration, the high selectivity for formic acid was maintained, demonstrating excellent stability.

Chapter Four

Formation of high entropy oxide anode by morphology remodeling for promoting oxygen evolution reaction

4.1 Introduction

The selectivity of various components in high-entropy materials can maximize the synergistic effects between different active sites and more effectively adjust the electronic structure, thereby optimizing the energy barriers in electrocatalytic processes and improving reaction performance, making it a very promising candidate for electrolytic fresh water and seawater splitting. The diffusion kinetics of HEAs are more sluggish than the ones in usual alloys since the adjacent atoms of HEMs at each lattice are discrepant, which can lead to different local bonding energies. In this case, if an atom stays at a low-energy position, it is in a stable state and difficult to move or be replaced. In contrast, when an atom is dragged away to a high-energy position, it will strive to jump back to the low-energy site. As such, the atoms of HEM will stay at the stable state and resist to reaction, thereby enhancing catalyst corrosion resistance [87].

The direct synthesis of high-entropy compounds needs overcoming issues related to the incompatibility of different elements, especially metals and non-metals. Lai et al. [136] utilized citric acid as the chelating agent to form a cross-linked network by connecting five metal ions, in which the metal ions can uniformly dispersed within the network, overcoming the incompatibility between different metals and non-metals. However, by using this method, it is difficult to grow the HEA electrocatalysts directly on the electrode, and the obtained material needs to be further coated onto the electrode surface, which will increase application costs and decrease the performance to some extent. In our group, a solvothermal method was used for synthesizing high-entropy MOF precursor on a nickel foam (NiF), which was further converted into an efficient high-entropy phosphide (HEP) for water electrolysis [137].

Herein, we report an intriguing phenomenon in the preparation of high-entropy FeCoNiMnCu based electrocatalysts. It is found that the high-entropy precursor with a layered fusiform architecture obtained by a hydrothermal process was transformed to a sphere-shape after the annealing while maintaining high-entropy characteristics. This transformation effectively enhanced the electrocatalytic performance, especially in the case of the resulting high-entropy oxide, (FeCoNiMnCu)O_x, which exhibited excellent OER activity. (FeCoNiMnCu)O_x as the anode for OER in alkaline seawater showed excellent stability with running continuously for 160 hours even at current densities exceeding 100 mA cm⁻², over the performance by using precious metal based electrocatalysts.

4.2 Experimental

The synthesis process involves several steps to treat Nickel foam (NiF) and deposit the precursor for subsequent conversion to high-entropy metal oxide (HEO).

4.2.1 Nickel Foam Treatment

Objective: The purchased Nickel foam was subjected to a treatment process to eliminate impurities and the superficial oxide layer.

Procedure: The NiF was immersed in an 3M HCl solution for this purpose.

Storage: After treatment, the NiF was stored in ethanol.

4.2.2 Precursor Deposition on NiF (Hydrothermal Method)

Ingredients: 2 mmol Mn(NO₃)₂, 1.5 mmol Co(NO₃)₂, 1.5 mmol Ni(NO₃)₂, 0.8 mmol Fe(NO₃)₃, 0.2 mmol Cu(NO₃)₂, 12 mmol urea, 6 mmol NH₄F, 30 mL distilled water

Procedure: Precursor was deposited on NiF by a hydrothermal method, in which a mixed solution of ingredients in the 30 mL distilled water was used and the hydrothermal reaction was conducted at 120 °C and 6 hours. In the Teflon-lined autoclave (50 mL) utilized for hydrothermal synthesis, two pieces of pre-treated NiF were used together.

4.2.3 Conversion to High-Entropy Oxide (HEO)

The precursor was subjected to thermal oxidation in a muffle furnace. The temperature was raised to 350 °C and held at this temperature for 2 hours. The ramp rate was set at 2 °C min⁻¹.

4.3 Results and Discussion

4.3.1 Morphology and Crystal Structure

As shown in Fig. 2(a-b), the high-entropy precursor exhibits a fusiform morphology with a length between 8 and 10 μm and a width between 2 and 5 μm. The XRD pattern indicates that the obtained precursor has a single-phase face-centered cubic (FCC) structure (Fig. 4.1e). While, in the fusiform interior, there are certain lattice fringes corresponding to the (111) plane of FCC (PDF#47-1450, 0.207 nm) with an interplanar distance of 0.209 nm (Fig.4.1b). It demonstrates the successful synthesis of high-entropy precursor. Whereafter, the precursor has been transformed to a spherical structure composed of a lamellar structure after the calcination treatment (Fig.4.1c-d). HEO have layer structure with sphere-like array, in which there is enough space among neighboring layers for the diffusion of gas and ions. In the complex electrolysis environment of alkaline seawater, it can prevent the deposition of pollutants effectively, thus improving stability. Herein, the morphology remodeling of high entropy precursor could be due to the atom decomposition and recombination during the calcination process. The sphere diameter ranges from 5 to 7 micrometers, and thicknesses of HEO are about 50 nm (Fig. 4.1)

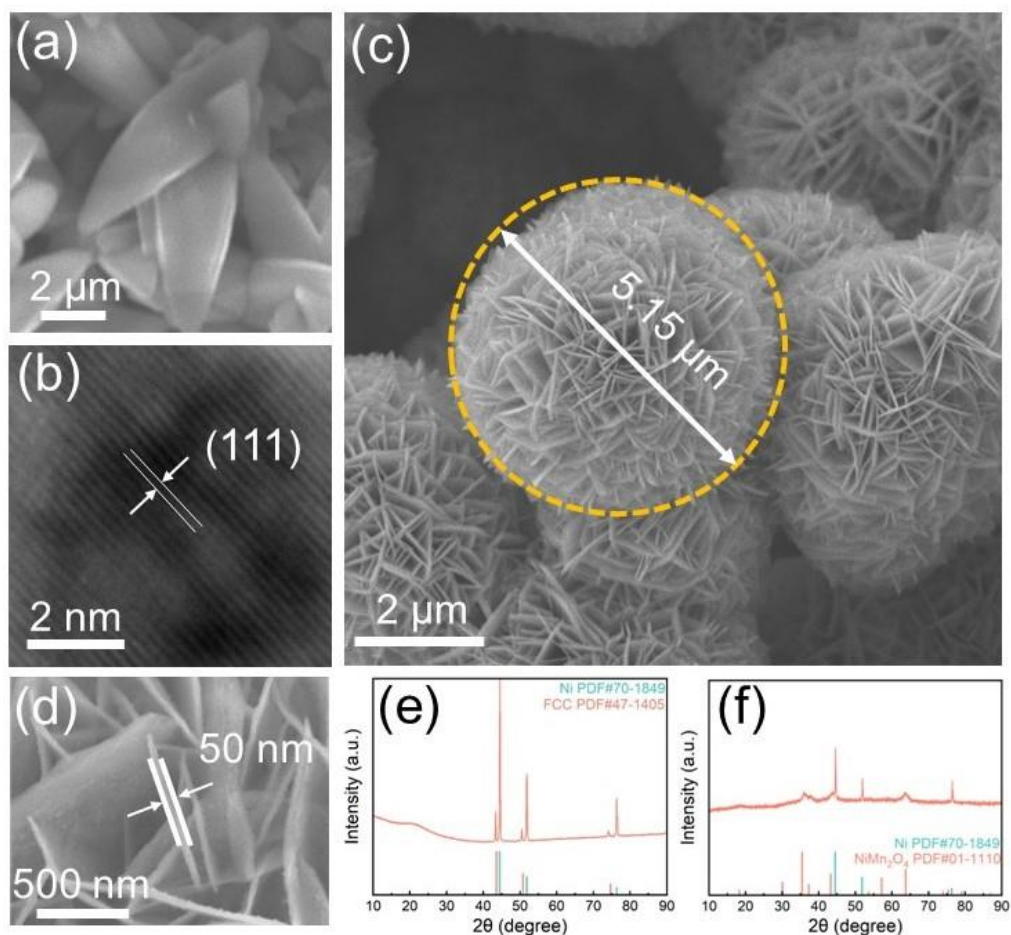


Fig. 4.1 SEM images of (a) (FeCoNiMnCu)-precursor and (c-d) (FeCoNiMnCu) O_x . TEM image of (b) (FeCoNiMnCu)-precursor. XRD patterns of (e) (FeCoNiMnCu)-precursor and (f) (FeCoNiMnCu) O_x .

The obtained (FeCoNiMnCu) O_x HEO exhibits a crystal structure akin to that of NiMn $2O_4$ (PDF#01-1110, Fig. 4.1f). While, in the (FeCoNiMnCu) O_x HEO, there are certain lattice fringes corresponding to the (400) plane of NiMn $2O_4$ (PDF#01-1110, 0.209 nm) with an interplanar distance of 0.208 nm (Fig. 3j). It should be attributed to the lattice distortion effect of high-entropy materials. Meanwhile, the obtained (FeCoNiMnCu) O_x HEO also displays a nanodot built nanolayer morphology (Fig. 4.2).

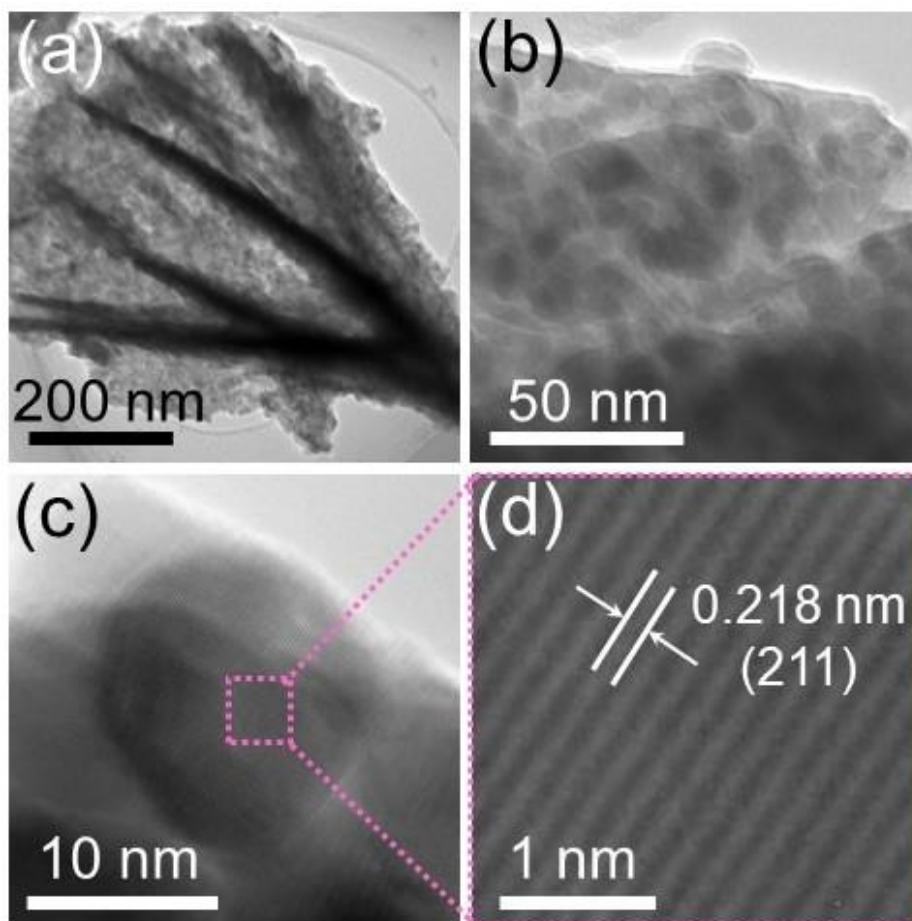


Fig. 4.2 TEM images of high-entropy $(\text{FeCoNiMnCu})\text{O}_x$.

4.3.2 The influence of composition on the morphologies and crystals

It is found that all the precursors with Fe, NiFe, FeCoNi, FeCoNiMn element groups have similar nanosheet microstructure with spherical array (Fig. 4.3).

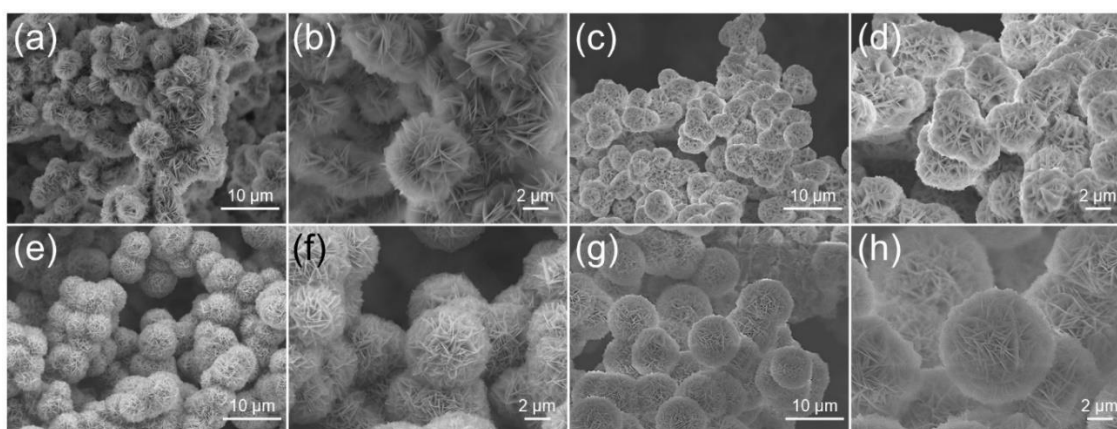


Fig. 4.3 SEM images of (a-b) Fe-precursor, (c-d) FeNi-precursor, (e-f) FeCoNi-precursor, and (g-h) FeCoNiMn-precursor.

Interestingly, XRD patterns (Figs. 4.4a) prove that and NiFe precursors display a similar crystal structure as NiFe LDH (layered double hydroxides) (PDF#40-0215) [138]. However, the FeCoNi precursor is combined by the mixture of multiple compounds (Figs. 4.4b), including NiFe LDH and Co₃O₄. Similarly, it can find that mixed crystal structures are close to NiFe LDH, MnO₂ and Co₃O₄ mixed compositions in FeCoNiMn precursor, which may be due to the weak combination ability of Co and Mn elements with the Ni, Fe elements (Figs. 4.4c). However, the FeCoNiMnCu precursor has a typical single crystal structure, which should be due to the high-entropy effect. Besides, the morphology FeCoNiMnCu precursor changes from sphere to fusiform after the addition of Cu²⁺ (Fig. 2a), which could be due to the rapid crystalline growth rate of Cu based species, which results in the formation of a larger bulk structure.

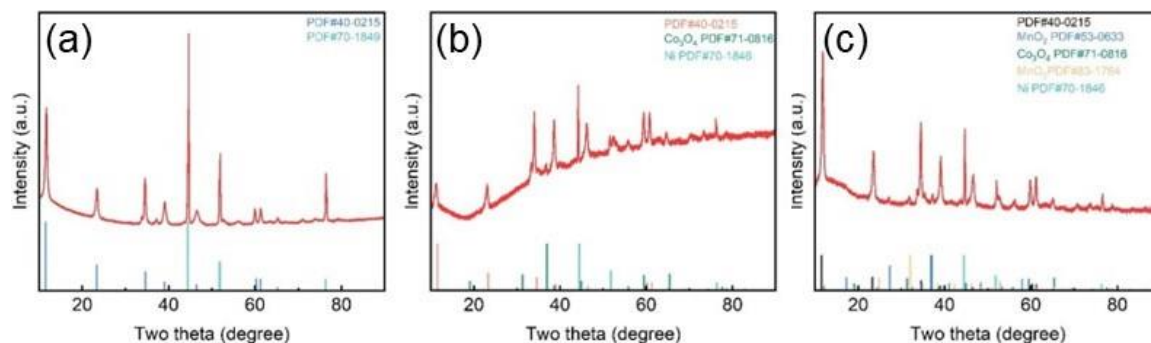


Fig. 4.4 XRD pattern of (a) NiFe-precursor, (b) FeCoNi-precursor and (c) FeCoNiMn-precursor.

4.3.3 Electrochemical test

Fig. 4.6(a) shows the LSV curves of different as-prepared electrodes for in seawater + 1 M KOH. Obviously, the (FeCoNiMnCu)Ox also reveals highest OER activity ($\eta_{20} = 363.3$ mV) due to the advantages of high entropy materials. Besides, the overpotential of NiFeO coated electrode is smaller than those of FeO, CoNiFeO, and MnCoNiFeO electrocatalyst coated ones, indicating the participant elements also play crucial role in adjusting catalytic activity. As shown in the Nyquist

plot (Fig. 4.6d), the (FeCoNiMnCu)O_x base electrode has a smaller semicircle diameter compared to the other four ones, indicating that the intermediate diffusion and conversion rate on this HEO are faster than the other ones. As shown in Fig. 4.6(e), the C_{dl} (99.5 mF cm⁻²) of this HEO is also large, only lower than that of FeO (116.3 mF cm⁻²), confirming that it has a larger electrochemical surface area. Moreover, the significantly higher performance compared to FeO proves that the active sites of (FeCoNiMnCu)O_x should be more active than those of FeO. In addition, after 160-hour of stability testing, the current density has no obvious change at 1.8 V (Fig. 4.6f).

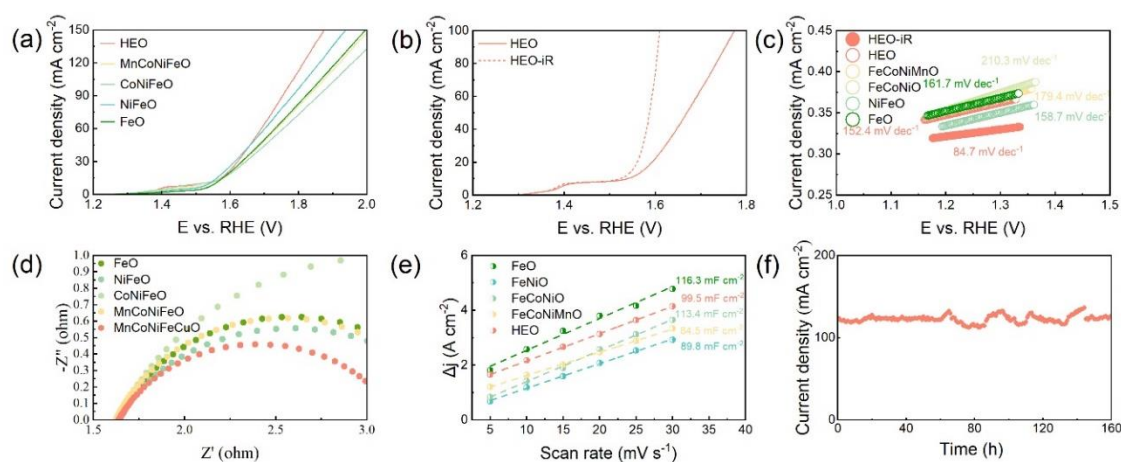


Fig. 4.6 Electrocatalytic performances in the OER evaluation: LSV curves of (a) FeO, NiFeO, FeCoNiO, FeCoNiMnO and (FeCoNiMnCu)O_x and (b) (FeCoNiMnCu)O_x with iR correction. (c) Tafel slopes, (d) EISs, and (e) C_{dl} values of different samples. (f) Chronoamperometry curve of (FeCoNiMnCu)O_x based electrode in seawater + 1 M KOH.

4.3.5 Conclusion

In summary, (FeCoNiMnCu)O_x electrocatalysts were synthesized by a facile hydrothermal process followed with oxidization. Especially, the morphology remodeling from FeCoNiCuMn-based high-entropy precursor to HEO were analysed, which converted from fusiform bulk architecture to a nanosheet structure with sphere array after the thermal oxidization process. Due to the large surface area and advantages of HEM catalysts, the obtained HEO demonstrated outstanding OER performance with overpotentials of 363 mV@20 mA cm⁻². HEO also showed excellent stability with running continuously for 160 hours at current densities even exceeding 120

mA cm⁻², which surpassed the performances of precious metal based electrocatalysts, offering the potential for low-cost and efficient seawater electrolysis.

Chapter Five

General conclusions

This study focuses on the development of a high-entropy metal-organic framework (MOF) as a cathode catalyst for the electrochemical CO₂RR, along with the synthesis of a high-entropy oxide for OER as an anode catalyst. The key findings from the experimental investigations are summarized as follows:

(1) A high-entropy metal-organic framework (HE-MOF) based on Bi, In, Sn, Pb, and Cu was synthesized and grown on carbon paper through a hydrothermal method. XRD analysis confirmed the formation of a high-entropy structure on CP, denoted as BiInSnPbCu-CP cathode. The catalyst demonstrated remarkable performance with high selectivity (over 80% Faradaic efficiency) and stability (20 hours) in the production of formic acid via the electrochemical reduction of carbon dioxide.

(2) A high-entropy precursor with a fusiform microstructure was employed to prepare (FeCoNiMnCu)Ox. Upon thermal oxidization, the microstructures of the resulting high-entropy (FeCoNiMnCu)Ox were transformed into a layered sphere-shaped microstructure composed of nanodots. The high-entropy oxide (HEO) exhibited excellent stability, running continuously for 160 hours at current densities exceeding 100 mA cm⁻², surpassing the performance of precious metal-based electrocatalysts.

(3) For the above two high-entropy electrocatalysts of cathodic and anode, because they have excellent performances, if assembled them into one electrolyzer, which could exhibit outstanding overall electrolysis performance for CO₂RR. I will continue to do this work.

References

- [1] S Jin, Z Hao, K Zhang, Z Yan, J Chen, Advances and challenges for the electrochemical reduction of CO₂ to CO: from fundamentals to industrialization. *Angewandte Chemie*. 13 (2021) 20795-20816.
- [2] F Pietrapertosa, M Salvia, S.D.G Hurtado, D Geneletti, V D'Alonzo, Diana Reckien, Multi-level climate change planning: An analysis of the Italian case. *Journal of environmental management*. 289 (2021) 112469.
- [3] M.E. Boot-Handford, J.C. Abanades, E.J. Anthony, M.J. Blunt, S Brandani, N.M. Dowell, J.R. Fernández, M.C. Ferrari, R Gross, J.P. Hallett, R.S. Haszeldine, P Heptonstall, A Lyngfelt, Z Makuch, E Mangano, R.T.J. Porter, M Pourkashanian, G.T. Rochelle, N Shah, J.I.G. Yao, P.S. Fennell, Carbon capture and storage update. *Energy & Environmental Science*. 7 (2014) 130-189.
- [4] S Fawzy, A.I. Osman, J Doran, D.W. Rooney, Strategies for mitigation of climate change: a review. *Environmental Chemistry Letters*. 18 (2020): 2069-2094.
- [5] C.J. Brigham, K Kurosawa, C Rha, A.J.Sinskey, Bacterial carbon storage to value added products. *Microb. Biochem. Technol*. 3 (2011) 002
- [6] P.R. Yaashikaa, P Senthil Kumar, S.J. Varjani, A. Saravanan, A review on photochemical, biochemical and electrochemical transformation of CO₂ into value-added products. *Journal of CO₂ Utilization*. 33 (2019) 131-147.
- [7] O Hakami, Thermocatalytic and solar thermochemical carbon dioxide utilization to solar fuels and chemicals: A review. *International Journal of Energy Research*. 14 (2022) 19929-19960.
- [8] Y Fan, J Ren, W Onstot, J Pasale, T.T. Tsotsis, F.N. Egolfopoulos, Reactor and technical feasibility aspects of a CO₂ decomposition-based power generation cycle, utilizing a high-temperature membrane reactor. *Industrial & engineering chemistry research*. 12 (2003) 2618-2626.

- [9] G.A. Olah, A Goeppert, G.K.S. Prakash, Chemical recycling of carbon dioxide to methanol and dimethyl ether: from greenhouse gas to renewable, environmentally carbon neutral fuels and synthetic hydrocarbons. *The Journal of organic chemistry*. 2 (2009) 487-498.
- [10] J.C. Navarro, M.A. Centeno, O.H. Laguna, J.A. Odriozola, Policies and motivations for the CO₂ valorization through the sabatier reaction using structured catalysts. A review of the most recent advances. *Catalysts*. 12 (2018) 578.
- [11] F.O. Ochedi, D Liu, J Yu, A Hussain, Y Liu, Photocatalytic, electrocatalytic and photoelectrocatalytic conversion of carbon dioxide: a review. *Environmental Chemistry Letters*. 19 (2021) 941-967.
- [12] H Liu, X Meng, T.D. Dao, H Zhang, P Li, K Chang, T Wang, M Li, T Nagao, J Ye, Conversion of carbon dioxide by methane reforming under visible-light irradiation: surface-plasmon-mediated nonpolar molecule activation. *Angewandte Chemie*. 39 (2015) 11707-11711.
- [13] X Song, X Li, X Zhang, Y Wu, C Ma, P Huo, Y Yan, Fabricating C and O co-doped carbon nitride with intramolecular donor-acceptor systems for efficient photoreduction of CO₂ to CO. *Applied Catalysis B: Environmental*. 268 (2020): 118736.
- [14] L Wang, P Jin, S Duan, H She, J Huang, Q Wang, In-situ incorporation of Copper (II) porphyrin functionalized zirconium MOF and TiO₂ for efficient photocatalytic CO₂ reduction. *Science bulletin*. 13 (2019) 926-933.
- [15] X Wang, X Zhao, D Zhang, G Li, H Li, Microwave irradiation induced UIO-66-NH₂ anchored on graphene with high activity for photocatalytic reduction of CO₂. *Applied Catalysis B: Environmental*. 228 (2018) 47-53.
- [16] A Sharma, B.K. Lee, Photocatalytic reduction of carbon dioxide to methanol using nickel-loaded TiO₂ supported on activated carbon fiber. *Catalysis Today*. 298 (2017) 158-167.

- [17] M Tahir, Photocatalytic carbon dioxide reduction to fuels in continuous flow monolith photoreactor using montmorillonite dispersed Fe/TiO₂ nanocatalyst. *Journal of Cleaner Production*. 170 (2018) 242-250.
- [18] G Song, F Xin, X Yin, Photocatalytic reduction of carbon dioxide over ZnFe₂O₄/TiO₂ nanobelts heterostructure in cyclohexanol. *Journal of colloid and interface science*. 442 (2015) 60-66.
- [19] M Li, M.N. Idros, Y Wu, T Burdyny, S Garg, X.S. Zhao, G Wang, T.E. Rufford, The role of electrode wettability in electrochemical reduction of carbon dioxide. *Journal of Materials Chemistry A*. 9 (2021): 19369-19409.
- [20] D Ewis, M Arsalan, M Khaled, D Pant, M.M. Ba-Abbad, A Amhamed, M.H. El-Naas, Electrochemical reduction of CO₂ into formate/formic acid: A review of cell design and operation. *Separation and Purification Technology*. (2023): 123811.
- [21] Y Liu, F Li, X Zhang, X Ji, Liu, Yanrong, et al. Recent progress on electrochemical reduction of CO₂ to methanol. *Current Opinion in Green and Sustainable Chemistry*. 23 (2020) 10-17.
- [22] Z Zhang, L Bian, H Tian, Y Liu, Y Bando, Y Yamauchi, Z.L. Wang, Tailoring the surface and interface structures of copper-based catalysts for electrochemical reduction of CO₂ to ethylene and ethanol. *Small*. 18 (2022) 2107450.
- [23] K Zhao, X Nie, H Wang, S Chen, X Quan, H Yu, W Choi, G Zhang, B Kim, J.G. Chen, Selective electroreduction of CO₂ to acetone by single copper atoms anchored on N-doped porous carbon. *Nature communications*. 11 (2020) 2455.
- [24] Y Yang, H Gao, J Feng, S Zeng, L Liu, L Liu, B Ren, T Li, S Zhang, X Zhang, Aromatic Ester-Functionalized Ionic Liquid for Highly Efficient CO₂ Electrochemical Reduction to Oxalic Acid. *ChemSusChem*. 13 (2020) 4900-4905.
- [25] S Ning, J Wang, D Xiang, S Huang, W Chen, S Chen, X Kang, Electrochemical reduction of SnO₂ to Sn from the Bottom: In-Situ formation of SnO₂/Sn heterostructure for highly efficient electrochemical reduction of carbon dioxide to formate. *Journal of Catalysis*. 399 (2021) 67-74.

- [26] Y Xiong, B Wei, M Wu, B Hu, F Zhu, J Hao, W Shi, Rapid synthesis of amorphous bimetallic copper-bismuth electrocatalysts for efficient electrochemical CO₂ reduction to formate in a wide potential window. *Journal of CO₂ Utilization*. 51 (2021) 101621.
- [27] H Xie, T Wang, J Liang, Q Li, S Sun, Cu-based nanocatalysts for electrochemical reduction of CO₂. *Nano Today*. 21 (2018) 41-54.
- [28] D Du, R Lan, J Humphreys, S Tao, Progress in inorganic cathode catalysts for electrochemical conversion of carbon dioxide into formate or formic acid. *Journal of Applied Electrochemistry*. 47 (2017) 661-678.
- [29] O Scialdone, A Galia, GL Nero, F Proietto, S Sabatino, B Schiavo, Electrochemical reduction of carbon dioxide to formic acid at a tin cathode in divided and undivided cells: effect of carbon dioxide pressure and other operating parameters. *Electrochimica Acta*. 199 (2016) 332-341.
- [30] D.A. Bulushev, J.R.H. Ross, Vapour phase hydrogenation of olefins by formic acid over a Pd/C catalyst. *Catalysis Today*. 163 (2011) 42-46.
- [31] S Sharma, D.S. Patle, A.P. Gadhamsetti, S Pandit, D Manca, G.S. Nirmla, Intensification and performance assessment of the formic acid production process through a dividing wall reactive distillation column with vapor recompression. *Chemical Engineering and Processing-Process Intensification*. 123 (2018) 204-213.
- [32] D.A. Bulushev, J.R.H. Ross, Towards sustainable production of formic acid." *ChemSusChem*. 11 (2018) 821-836.
- [33] Y Guan, X Zhang, Y Zhang, TNV Karsili, M Fan, Achieving high selectivity towards electro-conversion of CO₂ using In-doped Bi derived from metal-organic frameworks. *Journal of Colloid and Interface Science*. 612 (2022) 235-245.
- [34] J Wu, F.G. Risalvato, F.S. Ke, P.J. Pellechia, X.D. Zhou, Electrochemical reduction of carbon dioxide I. Effects of the electrolyte on the selectivity and activity with Sn electrode. *Journal of the Electrochemical Society*. 159 (2012) F353.

- [35] Y Qian, Y Liu, H Tang, B.L. Lin, Highly efficient electroreduction of CO₂ to formate by nanorod@2D nanosheets SnO. *Journal of CO₂ Utilization*. 42 (2020) 101287.
- [36] L.C. Weng, A.T. Bell, A.Z. Weber, Modeling gas-diffusion electrodes for CO₂ reduction. *Physical Chemistry Chemical Physics*. 20 (2018) 16973-16984.
- [37] K.P. Kuhl, E.R. Cave, D.N. Abram, T.F. Jaramillo, New insights into the electrochemical reduction of carbon dioxide on metallic copper surfaces. *Energy & Environmental Science*. 5 (2012) 7050-7059.
- [38] J.S. Yoo, R Christensen, T Vegge, J.K. Nørskov, F Studt, Theoretical insight into the trends that guide the electrochemical reduction of carbon dioxide to formic acid. *ChemSusChem*. 9 (2016): 358-363.
- [39] E Irtem, T Andreu, A Parra, MD Hernández-Alonso, S García-Rodríguez, JM Riesco-García, G. Penelas-Pérez, J. R. Morante, Low-energy formate production from CO₂ electroreduction using electrodeposited tin on GDE. *Journal of Materials Chemistry A*. 4 (2016): 13582-13588.
- [40] K Hara, A Kudo, T Sakata, Electrochemical reduction of carbon dioxide under high pressure on various electrodes in an aqueous electrolyte. *Journal of Electroanalytical Chemistry*. 391 (1995) 141-147.
- [41] J Medina-Ramos, JL DiMeglio, Joel Rosenthal, Efficient reduction of CO₂ to CO with high current density using in situ or ex situ prepared Bi-based materials. *Journal of the American Chemical Society*. 136 (2014) 8361-8367.
- [42] H Yang, N Han, J Deng, J Wu, Y Wang, Y Hu, P Ding, Y Li, Y Li, J Lu, Selective CO₂ reduction on 2D mesoporous Bi nanosheets. *Advanced Energy Materials*. 8 (2018) 1801536.
- [43] Q Gong, P Ding, M Xu, X Zhu, M Wang, J Deng, Q Ma, N Han, Y Zhu, J Lu, Z Feng, Y Li, W Zhou, Y Li, Structural defects on converted bismuth oxide nanotubes enable highly active electrocatalysis of carbon dioxide reduction. *Nature communications*. 10 (2019) 2807.

- [44] Y Zhang, C Cao, X.T. Wu, Q.L. Zhu, Three-dimensional porous copper-decorated bismuth-based nanofoam for boosting the electrochemical reduction of CO₂ to formate." *Inorganic Chemistry Frontiers*. 8 (2021) 2461-2467.
- [45] D Wu, J Zhang, MJ Cheng, Q Lu, H Zhang, Machine learning investigation of supplementary adsorbate influence on copper for enhanced electrochemical CO₂ reduction performance. *The Journal of Physical Chemistry C*. 125.28 (2021): 15363-15372.
- [46] Y Hori, Electrochemical CO₂ reduction on metal electrodes. *Modern aspects of electrochemistry*. (2008) 89-189.
- [47] Q Lai, N Yang, G Yuan, Highly efficient In–Sn alloy catalysts for electrochemical reduction of CO₂ to formate. *Electrochemistry Communications*. 83 (2017) 24-27.
- [48] X.L. Lu, X Rong, C Zhang, T.B. Lu, Carbon-based single-atom catalysts for CO₂ electroreduction: progress and optimization strategies. *Journal of Materials Chemistry A*. 8 (2020) 10695-10708.
- [49] A Del Castillo, M Alvarez-Guerra, A Irabien, Continuous electroreduction of CO₂ to formate using Sn gas diffusion electrodes. *AIChE Journal*. 60 (2014) 3557-3564.
- [50] A Del Castillo, M Alvarez-Guerra, J Solla-Gullón, A. Sáez, V. Montiel, A. Irabien, Electrocatalytic reduction of CO₂ to formate using particulate Sn electrodes: Effect of metal loading and particle size. *Applied Energy*. 157 (2015) 165-173.
- [51] V.S.K. Yadav, M.K. Purkait, Electrochemical reduction of CO₂ to HCOOH on a synthesized Sn electrocatalyst using a Co₃O₄ anode. *RSC Advances*. 5 (2015) 68551-68557.
- [52] T Tsujiguchi, Y Kawabe, S Jeong, T Ohto, S Kukunuri, H Kuramochi, Y Takahashi, T Nishiuchi, H Masuda, M Wakisaka, K Hu, G Elumalai, J Fujita, Y Ito, Acceleration of electrochemical CO₂ reduction to formate at the Sn/reduced graphene oxide interface. *ACS Catalysis*. 11 (2021) 3310-3318.

- [53] X Bai, W Chen, C Zhao, S Li, Y Song, R Ge, W Wei, Y Sun, Exclusive formation of formic acid from CO₂ electroreduction by a tunable Pd-Sn alloy. *Angewandte Chemie*. 129(2017) 12387-12391.
- [54] X An, S Li, A Yoshida, T Yu, Z Wang, X Hao, A Abudula, G Guan, Bi-doped SnO nanosheets supported on Cu foam for electrochemical reduction of CO₂ to HCOOH. *ACS applied materials & interfaces*. 11 (2019) 42114-42122.
- [55] Q Yang, Q Wu, Y Liu, S Luo, X Wu, X Zhao, H Zou, B Long, W Chen, Y Liao, L Li, PK Shen, L Duan, Z Quan, Novel Bi-doped amorphous SnO_x nanoshells for efficient electrochemical CO₂ reduction into formate at low overpotentials. *Advanced Materials*. 32 (2020) 2002822.
- [56] Y.F. Tay, Z.H. Tan, Y Lum, Engineering Sn-based catalytic materials for efficient electrochemical CO₂ reduction to formate. *ChemNanoMat*. 7.(2021) 380-391.
- [57] M Chen, S Wan, L Zhong, D Liu, H Yang, C Li, Z Huang, C Liu, J Chen, H Pan, D.S. Li, S Li, Q Yan, B Liu, Dynamic restructuring of Cu-doped SnS₂ nanoflowers for highly selective electrochemical CO₂ reduction to formate. *Angewandte Chemie*. 133 (2021) 26437-26441.
- [58] Y Hori, K Kikuchi, S Suzuki, Production of CO and CH₄ in electrochemical reduction of CO₂ at metal electrodes in aqueous hydrogencarbonate solution. *Chemistry letters*. 14 (1985) 1695-1698.
- [59] F Köleli, T Atilan, N Palamut, AM Gizir, R Aydin, CH Hamann, Electrochemical reduction of CO₂ at Pb-and Sn-electrodes in a fixed-bed reactor in aqueous K₂CO₃ and KHCO₃ media. *Journal of applied electrochemistry*. 33 (2003) 447-450.
- [60] B Innocent, D Liaigre, D Pasquier, F Ropital, JM Léger, KB Kokoh, Electro-reduction of carbon dioxide to formate on lead electrode in aqueous medium. *Journal of Applied Electrochemistry*. 39 (2009) 227-232.
- [61] C.H. Lee, M.W. Kanan, Controlling H⁺ vs CO₂ reduction selectivity on Pb electrodes. *Acs Catalysis*. 5 (2015) 465-469.

- [62] S.Y. Choi, S.K. Jeong, H.J. Kim, I.H. Baek, K.T. Park, Electrochemical reduction of carbon dioxide to formate on tin-lead alloys. *ACS Sustainable Chemistry & Engineering*. 4 (2016): 1311-1318.
- [63] V.S.K. Yadav, M.K. Purkait, Electrochemical studies for CO₂ reduction using synthesized Co₃O₄ (anode) and Cu₂O (cathode) as electrocatalysts. *Energy & Fuels*. 29 (2015) 6670-6677.
- [64] C.W. Li, M.W. Kanan, CO₂ reduction at low overpotential on Cu electrodes resulting from the reduction of thick Cu₂O films. *Journal of the American Chemical Society*. 134 (2012) 7231-7234.
- [65] Y Lan, C Gai, P.J.A. Kenis, J Lu, Electrochemical reduction of carbon dioxide on Cu/CuO core/shell catalysts. *ChemElectroChem*. 1 (2014) 1577-1582.
- [66] TN Huan, ES Andreiadis, J Heidkamp, P Simon, E Derat, S Cobo, G Royal, A Bergmann, P Strasser, H Dau, V Artero and M Fontecave, From molecular copper complexes to composite electrocatalytic materials for selective reduction of CO₂ to formic acid. *Journal of Materials Chemistry A*. 3 (2015) 3901-3907.
- [67] Y Wang, B Yu, M He, Z Zhai, K Yin, F Kong, Z Zhang, Eutectic-derived high-entropy nanoporous nanowires for efficient and stable water-to-hydrogen conversion. *Nano Research*. (2022) 1-7.
- [68] Y Lei, L Zhang, W Xu, C Xiong, W Chen, X Xiang, B Zhang, H Shang, Carbon-supported high-entropy Co-Zn-Cd-Cu-Mn sulfide nanoarrays promise high-performance overall water splitting. *Nano Research*. 15 (2022) 6054-6061.
- [69] Z Zhao, H Chen, H Xiang, F.Z. Dai, X Wang, Z Peng, Y Zhou, (La_{0.2}Ce_{0.2}Nd_{0.2}Sm_{0.2}Eu_{0.2}) PO₄: A high-entropy rare-earth phosphate monazite ceramic with low thermal conductivity and good compatibility with Al₂O₃. *Journal of Materials Science & Technology*. 35 (2019) 2892-2896.
- [70] H Chen, K Jie, CJ Jafta, Z Yang, S Yao, M Liu, Z Zhang, J Liu, M Chi, J Fu, S Dai, An ultrastable heterostructured oxide catalyst based on high-entropy materials: A new strategy toward

catalyst stabilization via synergistic interfacial interaction. *Applied Catalysis B: Environmental*. 276 (2020) 119155.

[71] J.W. Yeh, Alloy design strategies and future trends in high-entropy alloys. *Jom*. 65 (2013) 1759-1771.

[72] H Li, Y Huang, J Sun, Y Lu, The relationship between thermo-mechanical history, microstructure and mechanical properties in additively manufactured CoCrFeMnNi high entropy alloy. *Journal of Materials Science & Technology*. 77 (2021) 187-195.

[73] B Cantor, I.T.H. Chang, P Knight, A.J.B. Vincent, Microstructural development in equiatomic multicomponent alloys. *Materials Science and Engineering: A*. 375 (2004): 213-218.

[74] Z Lei, X Liu, Y Wu, H Wang, S Jiang, S Wang, X Hui, Y Wu, B Gault, P Kontis, D Raabe, L Gu, Q Zhang, H Chen, H Wang, J Liu, K An, Q Zeng, T Nieh, Z Lu, Enhanced strength and ductility in a high-entropy alloy via ordered oxygen complexes. *Nature*. 563.7732 (2018): 546-550.

[75] DB Miracle, ON Senkov, A critical review of high entropy alloys and related concepts. *Acta Materialia*. 122 (2017) 448-511.

[76] B Gludovatz, A Hohenwarter, D Catoor, E.H. Chang, E.P. George, R.O. Ritchie, A fracture-resistant high-entropy alloy for cryogenic applications. *Science*. 345 (2014) 1153-1158.

[77] G Zhang, K Ming, J Kang, Q Huang, Z Zhang, Xuerong Zheng, Xiaofang Bi, High entropy alloy as a highly active and stable electrocatalyst for hydrogen evolution reaction. *Electrochimica Acta*. 279 (2018) 19-23.

[78] X Chang, M Zeng, K Liu, L Fu, Phase engineering of high-entropy alloys. *Advanced Materials*. 32 (2020) 1907226.

[79] Sheng Guo, C.T. Liu, Phase stability in high entropy alloys: Formation of solid-solution phase or amorphous phase. *Progress in Natural Science: Materials International*. 21 (2011) 433-446.

- [80] Y Zhang, TT Zuo, Z Tang, MC Gao, KA Dahmen, Microstructures and properties of high-entropy alloys. *Progress in materials science*. 61 (2014) 1-93.
- [81] C.J. Tong, Y.L. Chen, J.W. Yeh, S.J. Lin, S.K. Chen, T.T. Shun, C.H. Tsau, S.Y. Chang, Microstructure characterization of Al_xCoCrCuFeNi high-entropy alloy system with multiprincipal elements. *Metallurgical and Materials Transactions A*. 36 (2005) 881-893.
- [82] H Wu, M Qin, W Wang, Z Cao, Z Liu, Q Yu, C Lao, D Zhang, B Jia, D He, T Liu, AA Volinsky, P Cao, X Qua, Ultrafast synthesis of amorphous VO_x embedded into 3D strutted amorphous carbon frameworks—short-range order in dual-amorphous composites boosts lithium storage. *Journal of Materials Chemistry A*. 6 (2018) 7053-7061.
- [83] Zhang, R Li, S Pang, Effect of similar elements on improving glass-forming ability of La–Ce-based alloys. *Journal of Alloys and Compounds*. 483 (2009) 60-63.
- [84] NLN Broge, M Bondesgaard, F Søndergaard-Pedersen, M Roelsgaard, BB Iversen, Autocatalytic formation of high-entropy alloy nanoparticles. *Angewandte Chemie*. 132 (2020) 22104-22108.
- [85] H Liu, L Syama, L Zhang, C Lee, C Liu, Z Dai, Q Yan, High-entropy alloys and compounds for electrocatalytic energy conversion applications. *SusMat*. 1 (2021) 482-505.
- [86] K Huang, B Zhang, J Wu, T Zhang, D Peng, X Cao, Z Zhang, Z Li, Y Huang, Exploring the impact of atomic lattice deformation on oxygen evolution reactions based on a sub-5 nm pure face-centred cubic high-entropy alloy electrocatalyst. *Journal of Materials Chemistry A*. 8 (2020) 11938-11947.
- [87] X Li, Y Zhou, C Feng, R Wei, X Hao, K Tang, G Guan, High entropy materials based electrocatalysts for water splitting: Synthesis strategies, catalytic mechanisms, and prospects. *Nano Research*. 16 (2023) 4411-4437.

- [88] S Ranganathan, Alloyed pleasures: Multimetallc cocktails. *Current science*. 85 (2003) 1404-1406.
- [89] J.W. Yeh, S.K. Chen, S.J. Lin, J.Y. Gan, T.S. Chin, T.T. Shun, C.H. Tsau, S.Y. Chang, Nanostructured high-entropy alloys with multiple principal elements: novel alloy design concepts and outcomes. *Advanced engineering materials*. 6 (2004) 299-303.
- [90] J Zhang, Y Hu, Q Wei, Y Xiao, P Chen, G Luo, Q Shen, Microstructure and mechanical properties of RexNbMoTaW high-entropy alloys prepared by arc melting using metal powders. *Journal of Alloys and Compounds*. 827 (2020) 154301.
- [91] V.V. Popov, A Katz-Demyanetz, A Koptuyug, M Bamberger, Selective electron beam melting of Al_{0.5}CrMoNbTa_{0.5} high entropy alloys using elemental powder blend. *Heliyon*. 5 (2019).
- [92] S Luo, C Zhao, Y Su, Q Liu, Z Wang, Selective laser melting of dual phase AlCrCuFeNi_x high entropy alloys: Formability, heterogeneous microstructures and deformation mechanisms. *Additive Manufacturing*. 31 (2020) 100925.
- [93] S Xiang, J Li, H Luan, A Amar, S Lu, K Li, L Zhang, X Liu, G Le, X Wang, F Qu, W Zhang, D Wang, Q Li, Effects of process parameters on microstructures and tensile properties of laser melting deposited CrMnFeCoNi high entropy alloys. *Materials Science and Engineering: A*. 743 (2019): 412-417.
- [94] X Li, Additive manufacturing of advanced multi-component alloys: bulk metallic glasses and high entropy alloys. *Advanced Engineering Materials*. 20 (2018) 1700874.
- [95] B Winkler, EA Juarez-Arellano, W Morgenroth, A Barkov, A.C. Dippel, M Zimmermann, O Ivashko, O Gutowski, Pt₂AuCuNiSn, a new noble metal single-phase high entropy alloy. *Journal of Solid State Chemistry*. 294 (2021) 121837.
- [96] Y Zhang, B Zhang, K Li, GL Zhao, SM Guo, Electromagnetic interference shielding effectiveness of high entropy AlCoCrFeNi alloy powder laden composites. *Journal of Alloys and Compounds*. 734 (2018) 220-228.

- [97] JK Pedersen, TAA Batchelor, A Bagger, Jan Rossmeisl, High-entropy alloys as catalysts for the CO₂ and CO reduction reactions. *ACS Catalysis*. 10 (2020) 2169-2176.
- [98] W Xu, H Chen, K Jie, Z Yang, T Li, S Dai, Entropy-driven mechanochemical synthesis of polymetallic zeolitic imidazolate frameworks for CO₂ fixation. *Angewandte Chemie International Edition*. 58 (2019): 5018-5022.
- [99] D Redka, C Gadelmeier, J Winter, M Spellauge, C Eulenkamp, P Calta, U Glatzel, J Minár, H.P. Huber, Sub-picosecond single-pulse laser ablation of the CrMnFeCoNi high entropy alloy and comparison to stainless steel AISI 304. *Applied Surface Science*. 544 (2021) 148839.
- [100] H.J. Qiu, G Fang, J Gao, Y Wen, J Lv, H Li, G Xie, X Liu, S Sun, Noble metal-free nanoporous high-entropy alloys as highly efficient electrocatalysts for oxygen evolution reaction. *ACS Materials Letters*. 1 (2019) 526-533.
- [101] Y Xin, S Li, Y Qian, W Zhu, H Yuan, P Jiang, R Guo, L Wang, High-entropy alloys as a platform for catalysis: progress, challenges, and opportunities. *ACS Catalysis*. 10 (2020) 11280-11306.
- [102] T Löffler, A Savan, A Garzón-Manjón, Michael Meischein, Christina Scheu, Alfred Ludwig, Wolfgang Schuhmann, Toward a paradigm shift in electrocatalysis using complex solid solution nanoparticles. *ACS Energy Letters*. 4.5 (2019) 1206-1214.
- [103] T Löffler, H Meyer, A Savan, P Wilde, A Garzón Manjón, YT Chen, E Ventosa, C Scheu, A Ludwig, W Schuhmann, Discovery of a multinary noble metal-free oxygen reduction catalyst. *Advanced Energy Materials*. 8 (2018) 1802269.
- [104] HY Wang, YY Hsu, R Chen, TS Chan, HM Chen, B Liu, Ni³⁺-induced formation of active NiOOH on the spinel Ni-Co oxide surface for efficient oxygen evolution reaction. *Advanced Energy Materials*. 5 (2015) 1500091.

- [105] Y Yao, Z Huang, P Xie, SD Lacey, RJ Jacob, H Xie, F Chen, A Nie, T Pu, M Rehwoldt, D Yu, Carbothermal shock synthesis of high-entropy-alloy nanoparticles. *Science*. 359 (2018) 1489-1494.
- [106] Y Xin, S Li, Y Qian, W Zhu, H Yuan, P Jiang, R Guo, L Wang, High-entropy alloys as a platform for catalysis: progress, challenges, and opportunities. *ACS Catalysis*. 10 (2020) 11280-11306.
- [107] M Bondesgaard, N.L.N. Broge, A Mamakhel, M Bremholm, B.B. Iversen, General solvothermal synthesis method for complete solubility range bimetallic and high-entropy alloy nanocatalysts. *Advanced Functional Materials*. 29 (2019) 1905933.
- [108] M Liu, Z Zhang, F Okejiri, S Yang, S Zhou, S Dai, Entropy-maximized synthesis of multimetallic nanoparticle catalysts via a ultrasonication-assisted wet chemistry method under ambient conditions. *Advanced Materials Interfaces*. 6 (2019) 1900015.
- [109] AL Wang, HC Wan, H Xu, YX Tong, GR Li, Quinary PdNiCoCuFe alloy nanotube arrays as efficient electrocatalysts for methanol oxidation. *Electrochimica Acta*. 127 (2014) 448-453.
- [110] D Tench, J White, Enhanced tensile strength for electrodeposited nickel-copper multilayer composites. *Metallurgical transactions A*. 15 (1984) 2039-2040.
- [111] S.G. Kwon, G Krylova, P.J. Phillips, R.F. Klie, S Chattopadhyay, T Shibata, E.E. Bunel, Y Liu, V.B. Prakapenka, B Lee, E.V. Shevchenko, Heterogeneous nucleation and shape transformation of multicomponent metallic nanostructures. *Nature materials*. 14.2 (2015) 215-223.
- [112] Y Yao, Z Huang, LA Hughes, J Gao, T Li, D Morris, SE Zeltmann, BH Savitzky, C Ophus, M. Minor, R Shahbazian-Yassar, L Hu, Extreme mixing in nanoscale transition metal alloys. *Matter*. 4 (2021) 2340-2353.
- [113] D Wu, K Kusada, T Yamamoto, T Toriyama, S Matsumura, I Gueye, O Seo, J Kim, S Hiroi, O Sakata, S Kawaguchi, Y Kubota, H Kitagawa, On the electronic structure and hydrogen evolution

reaction activity of platinum group metal-based high-entropy-alloy nanoparticles. *Chemical science*. 11 (2020) 12731-12736.

[114] B.H. Savitzky, L Hughes, K.C. Bustillo, H.D. Deng, N.L. Jin, E.G. Lomeli, W.C. Chueh, P Herring, A Minor, C Ophus, py4DSTEM: Open source software for 4D-STEM data analysis. *Microscopy and Microanalysis*. 25 (2019) 124-125.

[115] J Miao, P Ercius, SJL Billinge, Atomic electron tomography: 3D structures without crystals. *Science*. 353 (2016) 2157.

[116] Y Yang, J Zhou, F Zhu, Y Yuan, DJ Chang, DS Kim, M Pham, A Rana, X Tian, Y Yao, Stanley J. Osher, A.K. Schmid, L Hu, P Ercius, J Miao, Determining the three-dimensional atomic structure of an amorphous solid. *Nature*. 592 (2021) 60-64.

[117] J.K. Nørskov, T Bligaard, J Rossmeisl, C.H. Christensen, Towards the computational design of solid catalysts. *Nature chemistry*. 1 (2009) 37-46.

[118] M.C. Tropsch, J.R. Morris, P.R.C. Kent, A.R. Lupini, G.M. Stocks, Criteria for predicting the formation of single-phase high-entropy alloys. *Physical Review X*. 5 (2015) 011041.

[119] N.T. Suen, S.F. Hung, Q Quan, N Zhang, Y.J. Xu, H.M. Chen, Electrocatalysis for the oxygen evolution reaction: recent development and future perspectives. *Chemical Society Reviews*. 46 (2017) 337-365.

[120] M.M. Ayyub, M Chhetri, U Gupta, A Roy, C.N.R. Rao, Photochemical and photoelectrochemical hydrogen generation by splitting seawater. *Chemistry—A European Journal*. 24 (2018) 18455-18462.

[121] X Niu, Q Tang, B He, P Yang, Robust and stable ruthenium alloy electrocatalysts for hydrogen evolution by seawater splitting. *Electrochimica Acta*. 208 (2016) 180-187.

[122] L Yu, Q Zhu, S Song, B McElhenny, D Wang, C Wu, Z Qin, J Bao, Y Yu, S Chen, Z Ren, Non-noble metal-nitride based electrocatalysts for high-performance alkaline seawater electrolysis. *Nature communications*. 10 (2019) 5106.

- [123] W Tong, M Forster, F Dionigi, S Dresp, R Sadeghi Erami, P Strasser, AJ Cowan, P Farràs, Electrolysis of low-grade and saline surface water. *Nature Energy*. 5 (2020) 367-377.
- [124] J Song, C Wei, ZF Huang, C Liu, L Zeng, X Wang, ZJ Xu, A review on fundamentals for designing oxygen evolution electrocatalysts. *Chemical Society Reviews*. 49 (2020) 2196-2214.
- [125] X Cui, B Zhang, C Zeng, S Guo, Electrocatalytic activity of high-entropy alloys toward oxygen evolution reaction. *Mrs Communications*. 8 (2018) 1230-1235.
- [126] B Zhang, X Zheng, O Voznyy, R Comin, M Bajdich, M García-Melchor, L Han, J Xu, M Liu, Homogeneously dispersed multimetal oxygen-evolving catalysts. *Science*. 352 (2016) 333-337.
- [127] N.B. Halck, V Petrykin, P Krtil, J Rossmeisl, Beyond the volcano limitations in electrocatalysis–oxygen evolution reaction. *Physical Chemistry Chemical Physics*. 16(2014) 13682-13688.
- [128] S Jin, Are metal chalcogenides, nitrides, and phosphides oxygen evolution catalysts or bifunctional catalysts? *ACS Energy Letters*. 2 (2017) 1937-1938.
- [129] B Song, Y Yang, M Rabbani, TT Yang, K He, X Hu, , Y Yuan, P Ghildiyal, V.P. Dravid, M.R. Zachariah, W.A. Saidi, Y Liu, R Shahbazian-Yassar, In situ oxidation studies of high-entropy alloy nanoparticles. *ACS nano*. 14 (2020): 15131-15143.
- [130] M.R. Chellali, A Sarkar, S.H. Nandam, S.S. Bhattacharya, B Breitung, H Hahn, L Velasco, On the homogeneity of high entropy oxides: An investigation at the atomic scale. *Scripta Materialia*. 166 (2019) 58-63.
- [131] A Sarkar, Q Wang, A Schiele, MR Chellali, SS Bhattacharya, D Wang, T Brezesinski, H Hahn, L Velasco, B Breitung, High-entropy oxides: fundamental aspects and electrochemical properties. *Advanced Materials*. 31 (2019) 1806236.

- [132] S Nellaiappan, NK Katiyar, R Kumar, A Parui, K.D. Malviya, K. G. Pradeep, A.K. Singh, S Sharma, C.S. Tiwary, K Biswas, High-entropy alloys as catalysts for the CO₂ and CO reduction reactions: Experimental realization. *ACS catalysis*. 10 (2020) 3658-3663.
- [133] T.A. Shifa, A Vomiero, Confined catalysis: progress and prospects in energy conversion. *Advanced Energy Materials*. 9 (2019) 1902307.
- [134] M Bondesgaard, N.L.N Broge, A Mamakhel, M Bremholm, B.B. Iversen, General solvothermal synthesis method for complete solubility range bimetallic and high-entropy alloy nanocatalysts. *Advanced Functional Materials*. 29 (2019) 1905933.
- [135] S Wang, W Huo, F Fang, Z Xie, JK Shang, J Jiang, High entropy alloy/C nanoparticles derived from polymetallic MOF as promising electrocatalysts for alkaline oxygen evolution reaction. *Chemical Engineering Journal*. 429 (2022): 132410.
- [136] D Lai, Q Kang, F Gao, Q Lu, High-entropy effect of a metal phosphide on enhanced overall water splitting performance. *Journal of Materials Chemistry A*. 9 (2021) 17913-17922.
- [137] Y Zhou, L Gao, H Chen, H Wang, J Zhang, X Li, F Duo, G Guan, Fabrication of amorphous FeCoNiCuMnP_x high-entropy phosphide/carbon composites with a heterostructured fusiform morphology for efficient oxygen evolution reaction. *Journal of Materials Science & Technology*. 168 (2024) 62-70.
- [138] J Wang, S Niu, T Guo, H Kou, J Li, The FCC to BCC phase transformation kinetics in an Al₁₀5CoCrFeNi high entropy alloy. *Journal of Alloys and Compounds*. 710 (2017) 144-150.

Acknowledgements

I extend my heartfelt appreciation to all researchers who have played a vital role in the successful completion of this thesis. Your contributions have been invaluable, and I am sincerely grateful for your dedication and support.

I would like to express my utmost gratitude to Professor Guoqing Guan, my advisor, for his invaluable guidance, unwavering support, and insightful suggestions that significantly contributed to the completion of this research. His expertise and encouragement played a pivotal role in shaping and refining this study. Additionally, I extend my thanks to Professor Abuliti Abudula for the support and assistance in both my research and daily life. Their contributions have been instrumental, and I am truly grateful for their mentorship.

I am grateful to Energy Conversion Engineering Laboratory for providing access to their state-of-the-art facilities and research resources, which greatly facilitated the experimental aspects of my work. The collaborative efforts of Ms Changrui Feng, Mr Ziyuan Yang and Ms Xiaohan Wu were instrumental in enhancing the overall quality of the research.

I would like to extend special thanks to Dr Meng Chen and Dr Yang He for their valuable academic exchange and camaraderie, which added a vibrant dimension to my research experience. Their contributions and collaboration were truly appreciated. Additionally, heartfelt gratitude goes to my friends and family for their unwavering support and encouragement throughout the entire research process. Their backing is invaluable, and I am grateful for their constant encouragement.

I express my gratitude to all those who have supported and assisted me silently, contributing to my academic journey in various ways. Their contributions have not gone unnoticed, and I am thankful for their silent but significant impact on my research and academic endeavors.

I hereby convey my deepest thanks to everyone who has been part of this journey.

List of publications and presentations

Presentations

1. **Yifan Zhou**, Changrui Feng, Meng Chen, Juan Zhang, Abuliti Abudula and Guoqing Guan, "Development of MnCo-based electrocatalysts for seawater splitting," International Symposium for the 80th Anniversary of the Tohoku Branch of the Chemical Society of Japan, Aobayama Commons, Tohoku University, Sendai, September 8-10, 2023.
2. **Yifan Zhou**, Abuliti Abudula, Guoqing Guan and Yasuki Kansha, "アルカリ海水分解用 $Mn_2Co_{1.5}Ni_{1.5}Fe_{0.8}Cu_{0.2}$ ベース高エントロピー電極触媒の開発", The Society of Chemical Engineers, Japan (SCEJ) 88th Annual Meeting, Tokyo, Japan, March 15-17, 2023.

Publications

1. **Yifan Zhou**, Longqing Gao, Haoyuan Chen, Hao Wang, Juan Zhang, Xiumin Li, Fangfang Duo and Guoqing Guan, "Fabrication of amorphous $FeCoNiCuMnP_x$ high-entropy phosphide/carbon composites with a heterostructured fusiform morphology for efficient oxygen evolution reaction," *Journal of Materials Science & Technology*, 168 (2024) 62-70.
2. Xiumin Li, **Yifan Zhou**, Changrui Feng, Ran Wei, Xiaogang Hao, Keyong Tang and Guoqing Guan, "High entropy materials based electrocatalysts for water splitting: Synthesis strategies, catalytic mechanisms, and prospects," *Nano Research*. 16 (2023) 4411-4437.
3. Changrui Feng, Meng Chen, **Yifan Zhou**, Zhengkun Xie, Xiumin Li, Pairuzha Xiaokaiti, Yasuki Kansha, Abuliti Abudula and Guoqing Guan, "High-entropy $NiFeCoV$ disulfides for enhanced alkaline water/seawater electrolysis," *Journal of Colloid and Interface Science*, 645 (2023) 724-734.
4. Nutthaphak Kitiphatpiboon, Meng Chen, Changrui Feng, **Yifan Zhou**, Changlin Liu, Zhongbao Feng, Qiang Zhao, Abuliti Abudula and Guoqing Guan, "Modification of spinel $MnCo_2O_4$

nanowire with NiFe-layered double hydroxide nanoflakes for stable seawater oxidation,” *Journal of Colloid and Interface Science*, 632 (2021) 54-64.